HHS Public Access

Author manuscript

J Control Release. Author manuscript; available in PMC 2024 December 01.

Published in final edited form as:

J Control Release. 2023 December ; 364: 109–123. doi:10.1016/j.jconrel.2023.10.028.

Catalytic antioxidant nanoparticles mitigate secondary injury progression and promote functional recovery in spinal cord injury model

Hayder Jaffer[1,†], **Syed Suhail Andrabi**[1,†], **Marianne Petro**[1,†], **Youzhi Kuang**[1], **Michael P. Steinmetz**[2], **Vinod Labhasetwar**[1,*]

[1]Department of Biomedical Engineering, Lerner Research Institute, Cleveland Clinic, Cleveland, OH 44195, USA

[2]Department of Neurosurgery, Neurological Institute, Cleveland Clinic, Cleveland, OH 44195, USA

Abstract

Traumatic spinal cord injury exacerbates disability with time due to secondary injury cascade triggered largely by overproduction of reactive oxygen species (ROS) at the lesion site, causing oxidative stress. This study explored nanoparticles containing antioxidant enzymes (antioxidant NPs) to neutralize excess ROS at the lesion site and its impact. When tested in a rat contusion model of spinal cord injury, a single dose of antioxidant NPs, administered intravenously three hours after injury, effectively restored the redox balance at the lesion site, interrupting the secondary injury progression. This led to reduced spinal cord tissue inflammation, apoptosis, cavitation, and inhibition of syringomyelia. Moreover, the treatment reduced scar tissue forming collagen at the lesion site, protected axons from demyelination, and stimulated lesion healing, with further analysis indicating the formation of immature neurons. The ultimate effect of the treatment was improved motor and sensory functions and rapid post-injury weight loss recovery. Histological analysis revealed activated microglia in the spinal cord displaying rod-shaped anti-inflammatory and regenerative phenotype in treated animals, contrasting with amoeboid inflammatory and degenerative phenotype in untreated control. Overall data suggest that restoring

[*]**Correspondence:** Vinod Labhasetwar, Ph.D., Department of Biomedical Engineering/ND20, Cleveland Clinic, 9500 Euclid Ave., Cleveland, OH 44195, Phone: 216-445-9364; Fax: 216-444-9198; labhasv@ccf.org.

[†]HJ, SA, and MP contributed equally to this study.

Author's contribution: JH: Animal studies, behavior, imaging, initial data collection, and analysis; **SA:** Animal study, antioxidant NP characterization, behavior study, MRI imaging, data analysis, and manuscript writing; **MP:** Behavior study, immunohistochemical staining, and data analysis of spinal tissue, **YK:** Antioxidant NP formulation and characterization; **MS:** Animal model and guidance, data review, and **VL:** Conceptualization, study design and supervision, data analysis and interpretation, and manuscript writing.

Conflict of Interest: HJ and VL are co-inventors on the US (#11,439,690) and EU (#2953640) patents that cover antioxidant NPs and their use for treating spinal cord injury. The technology is licensed to AxoNeural Therapeutics, Inc., a spinout company of Cleveland Clinic. VL is the founder of the company. The Conflict of Interest Committee of Cleveland Clinic manages the conflict of interest as per its conflict of interest policies.

Data and materials availability: All data are included in the main text. Nanoparticle formulations described in the manuscript will be made available to interested investigators under the material transfer agreement for research purposes.

the redox balance at the lesion site shifts the dynamics in the injured spinal cord microenvironment from degenerative to regenerative, potentially by promoting endogenous repair mechanisms. Antioxidant NPs show promise to be developed as an early therapeutic intervention in stabilizing injured spinal cord for enhanced recovery.

Graphical abstract

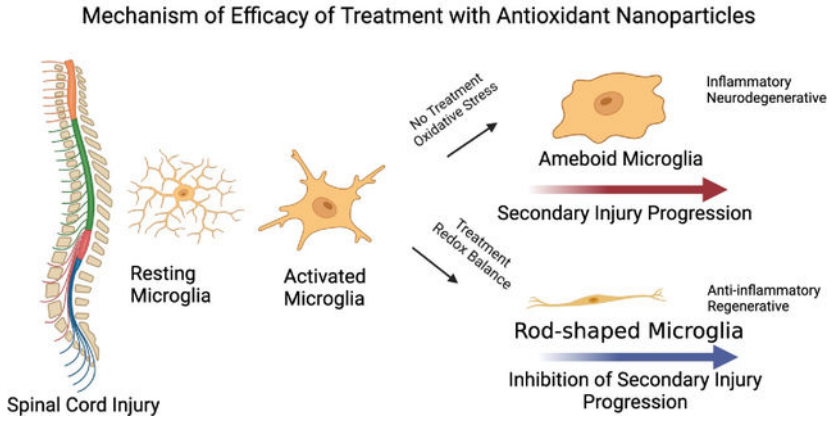

Keywords

Oxidative Stress; Free Radicals; Neurodegeneration; Biodegradable Polymer; Drug Delivery

1. Introduction

Traumatic spinal cord injury (SCI) involves primary and secondary injuries. Primary injury is caused by physical impact/trauma that immediately damages the spinal cord tissue at the impacted site. The initial injury rapidly activates progressive degenerative events known as “secondary injury” that expands the initial lesion site and, with time, affects the entire spinal cord [1]. This progressive degeneration of the injured spinal cord not only increases the level of disability with time but also diminishes the prospect of achieving neurological and functional recovery [2]. An effective intervention that can interrupt the cascade of secondary injury progression and stabilize the injured spinal cord from progressive degeneration is sorely needed [3].

Although few mechanisms of secondary injury progression are proposed [4], the one that we considered critical during the acute phase (acute <3 hours, subacute <24 hours) is the excessive reactive oxygen species (ROS) formation at the lesion site. The ROS-mediated damage to the cell-membrane lipids, proteins, and DNA, affecting critical cellular functions, triggers a cascade of degenerative events, causing inflammation and overexpression of apoptotic factors, resulting in further spinal tissue death [5, 6]. After the injury, dysfunctional mitochondria affect metabolic activities of the spinal cord cells/tissue and become the source of ROS [7], thus contributing to the vicious, self-propagating cycle of spinal cord tissue damage.

We considered the following criteria while developing an effective early therapeutic intervention for SCI. An injectable for intravenous administration as soon as possible after the injury, including at the trauma site, during transit to a trauma center, or immediately after post-hospitalization to minimize the impact of the initial injury. Given the limited holding capacity of the lesion cavity, the treatment should be highly effective even at low doses to ensure that it can neutralize the excess ROS formed at the lesion site. A sustained therapeutic effect at the lesion site is also essential, as is a broad therapeutic index to ensure that the treatment is nontoxic in a wide dose range and has a wide time window for treatment.

In this regard, natural and synthetic antioxidants, anti-inflammatory, or neuroprotective drugs have been evaluated but found ineffective in inhibiting secondary injury progression because of their low bioavailability, instability, limited transport to the lesion site, and transient retention [8]. In addition, antioxidants such as vitamins, flavonoids, antioxidant mimetics, etc., have very low antioxidant capacity. After interacting with ROS, antioxidant compounds/mimetics become inactive; hence, their therapeutic levels drop rapidly [9]. Repeated and high dosing of antioxidant compounds to maintain their therapeutic levels at the lesion site is challenging in clinical translation because of the toxicity concerns [10]. In line with that, high and frequent dosing of Vitamin E has been reported to increase the risk of mortality [11].

Antioxidant enzymes are highly potent in neutralizing ROS because of their catalytic mechanism of action; hence, they are effective even at low doses. Under normal physiological conditions, these endogenous antioxidant enzymes in cells and tissue maintain the redox balance by instantly neutralizing the ROS formed as a part of normal metabolic activities [12]. However, exogenously administered antioxidant enzymes, such as superoxide dismutase (SOD) and catalase (CAT), have very short half-lives as they are rapidly cleared via glomerular filtration (half-life = 8–11 min) [13], hence are ineffective in mitigating ROS [14]. PEGylation improves the circulation half-life of antioxidant enzymes to ~40 hours, but PEG interferes with their extravasation from the circulation into the target tissue [15]. In addition, at a cellular level, PEGylation affects intracellular uptake and endosomal escape for cytoplasmic delivery of antioxidant enzymes where ROS are primarily formed [16].

Encapsulation of antioxidant enzymes in nanoparticles (antioxidant NPs) protects them from rapid degradation and clearance, sustains their antioxidant effects, and facilitates cellular and tissue uptake [17, 18]. In our initial studies, at a cellular level, antioxidant NPs demonstrated protective effects against hydrogen peroxide-induced oxidative stress in neurons and astrocytes where antioxidant enzymes in solution or their PEGylated form were ineffective [16, 18]. In neurons, the treatment with antioxidant NPs reduced protein oxidation, DNA damage, mitochondrial membrane transition pore opening, and loss of cell membrane integrity [18]. In a rat contusion SCI model study, we determined that intravenously injected NPs localize in a dose-dependent manner and are retained at the lesion site, forming a depot [19]. In the subsequent investigation, we demonstrated that the treatment with antioxidant NPs attenuates the post-injury mitochondrial dysfunction and downregulates overexpression of the post-injury apoptotic factors, thus protecting the spinal cord tissue from apoptosis [20]. In this study, we hypothesized that the delivery of

antioxidant NPs neutralizes the excess ROS formed at the lesion site, thus regaining the redox balance, and protecting the injured spinal cord from secondary injury progression, leading to improved functional recovery.

2. Materials and Methods

2.1 Materials:

Poly (D,L-lactide *co*-glycolide) (PLGA; 50:50, inherent viscosity = 0.76–0.94 dL/g) was purchased from LACTEL Absorbable Polymers, now Evonik Corporation (Birmingham, AL). Poly (vinyl alcohol) (PVA; 87–90% hydrolyzed, mol. wt. 30,000–70,000), Dimethyl tartaric acid (DMT), Evans Blue (EB), Rat Serum Albumin (RSA), Superoxide Dismutase (SOD) from bovine red blood cells, and Catalase (CAT) from the bovine liver were purchased from Sigma-Aldrich (St. Louis, MO). Methylene chloride/Chloroform of HPLC grade was obtained from Fisher Scientific (Pittsburgh, PA). Near-infrared dye (NIR, SDB5700) was obtained from H.W. Sands Corp. (Jupiter, FL).

2.2 Formulation of Antioxidant and Near-infrared Dye-loaded Nanoparticles:

Antioxidant NPs were formulated by a double water-in-oil-in-water (w/o/w) emulsion solvent-evaporation method per the protocol described in our previous study [20]. Before their use, enzymatic activities of SOD and CAT were measured using the respective assay kits (SOD, Dojindo Molecular Technologies, Inc. Rockville, MD, and CAT, Sigma-Aldrich). The catalytic activity of SOD was ~5600 U/mg protein, and that of CAT was ~4800 U/mg protein. It has to be noted that SOD obtained from Sigma contains 95% protein, whereas CAT contains 55% protein (per product catalog information). We confirmed that there is no interference of SOD on the CAT assay and vice versa. In a typical preparation, each enzyme solution (8 mg CAT + 22 mg RSA or 12 mg SOD + 18 mg RSA dissolved in 300 μl of water) was emulsified into the polymer solution (81 mg PLGA + 9 mg DMT in 3 mL methylene chloride or chloroform) to form w/o emulsion. The amount of SOD or CAT specified in the above formulation is based on the weight of the products obtained from Sigma, not their protein content. The primary emulsion was further emulsified into a PVA solution (3% w/v PVA solution in water, 18 mL) to form a multiple (w/o/w) emulsion. RSA provides stability to the encapsulated enzymes from interfacial inactivation, and DMT, a pore-forming agent, facilitates the release of the encapsulated enzymes [17]. Following evaporation of the organic solvent, the formed NPs were recovered by ultracentrifugation; the supernatant and washings from the batch preparation were saved for quantifying the unencapsulated antioxidant enzymes using the respective enzymatic assay kits. In a few instances, they were prepared separately, reconstituted, and mixed before administration. In other instances, they were mixed following evaporation of the organic solvent and before lyophilization. In such cases, 1X batch of SOD-NPs and 2X batch of CAT-NPs were prepared separately and combined. Control NPs were prepared as above but contained only RSA. Near-infrared (NIR) dye-loaded NPs were prepared similarly to control NPs, but the dye was dissolved in the polymer solution before emulsification. The incorporated NIR dye acts as a marker for NPs and provides a quantitative signal proportional to the concentration of NPs [19].

2.3 Characterization of NPs:

Hydrodynamic diameter and zeta potential of antioxidant NPs and control/dye-loaded NPs were determined using NICOMP 380 ZLS (Particle Sizing Systems, Port Richey, FL). A stock dispersion of lyophilized antioxidant NPs was prepared in MQ water (2 mg/ml). Three μl of the above stock was diluted to 0.5 ml in MQ water for measuring particle size, and 100 μl of the stock was diluted to 3 ml in MQ water for measuring zeta potential. NP size was measured at a scattering angle of 90° at 25 °C, and zeta potential in phase-analysis mode at a scattering angle of −14°. Antioxidant NPs were further characterized by transmission electron microscopy (TEM). The encapsulation efficiency of each enzyme was determined from the difference in the amount added in the formulation and the amount seen in the supernatant and washings (unencapsulated). We used this indirect method to determine encapsulation efficiency, as direct extraction of enzymes/proteins from NPs using organic solvents leads to their inactivation/denaturation and incomplete recovery [17]. Using the indirect method and the respective assay kits to determine enzymatic activities, the encapsulation efficiency of SOD was 73% that of CAT was 85%. Previously, we determined sustained release of the encapsulated antioxidant enzymes in a buffer containing albumin at 37 °C [20].

2.4 Rat Contusion Model of SCI:

The Cleveland Clinic's Institutional Animal Care and Use Committee approved the animal procedures. These studies were carried out according to the Federal and internal guidelines. Sprague-Dawley rats (male/female) 6 to 8 weeks old were used (Harlan Laboratories, Indianapolis, IN, or Envigo, Cleveland, OH). The spinal cord was exposed by laminectomy at the T10 vertebrae level. Contusion injury was induced by utilizing a Kopf weight drop spinal compression apparatus with a 10 g weight dropped from a height of 25 mm (David Kopf Instruments, Tujunga, CA), inducing moderate SCI. The rat contusion model mimics many aspects of the human SCI [21]; hence, it is considered an adequate animal model for research on functional and morphological changes after SCI and to determine the effects of new treatment strategies [22].

2.5 Treatments:

Following SCI, a dose of 30 mg/kg dye-loaded NPs in 0.8 ml normal saline was administered intravenously at 3-, 6-, or 24 hours post-injury to determine their localization at the lesion site 24 hours after administration of NPs. The same dose of antioxidant NPs (30 mg/kg) was administered 3 hours post-injury to evaluate the treatment effect. The 30 mg/kg dose of antioxidant NPs contains a combination of 10 mg SOD-NPs and 20 mg CAT-NPs, or ~3800 Units (or ~690 μg SOD based on protein content) and ~3,000 Units (or 620 μg of CAT based on the protein content). These calculations also considered the encapsulation efficiencies of each enzyme, as mentioned above (Section 2.3). Based on the Units, the ratio of SOD: CAT is approximately 1:1 in antioxidant NPs. Other control groups were an equivalent dose of antioxidant enzymes in solution (ENZ), control NPs (without antioxidant enzymes), and saline control.

2.6 Harvesting of Spinal Cord:

Following euthanasia, animals were perfused via cardiac puncture with saline or 4% paraformaldehyde (PFA, Santa Cruz, Dallas, TX). The laminectomy was performed to isolate spinal cords. In a few experiments, the isolated spinal cords were further fixed in a PFA solution. Depending upon the objective, spinal cords were photographed, imaged using Maestro Optical Imaging, analyzed *in situ* by MRI, or processed for histological analysis.

2.7 Maestro Optical Imaging:

We explored Maestro Optical Imaging System (Version 3.0.1, Caliper Life Sciences, Hopkinton, MA) to determine the blood-spinal cord barrier (BSCB) leakage after the injury, localization of NPs at the lesion site, and ROS activity at the lesion site. The system has unique features to optimize wavelengths to detect a specific dye signal in the fluorescence or near-infrared range. Exposure times are optimized to prevent signal oversaturation to maintain a linear correlation between the signal and the amount of dye or dye-loaded NPs. The Maestro software creates spectra for the dye in experimental tissue and separately for the background in control tissue. The dye and the background signals can be segregated even if there is a minor variation in the spectra. The software can unmix the two spectral signals to create images exclusively due to the dye signal, which can be quantified. Apart from the above, SCI causes hemorrhage at the lesion site; however, the wavelength to capture the dye signals in the NIR region (740–950 nm) is beyond the wavelength range of hemoglobin (590–650 nm). In our experiment groups, the dye signals were captured using the NIR filter, whereas the background signal was captured using the blue filter (wavelength 500–720 nm).

Our previous study demonstrated that multiple dyes in the same tissue sample can be identified from the spectra and tagged for the respective dye. The images can be created for each dye separately, or they could be overlapped. We used this strategy to study biodistribution and co-localization of small- and large-sized NPs that were injected together but contained two different NIR dyes [23]. The Maestro method is quantitative and sensitive, and the signal correlates to the amount of dye or NPs in the tissue. The signal from homogenized tissue samples can also be quantified using a standard plot with different amounts of NPs added in the control tissue homogenate. Using the above method, we previously quantified NPs accumulation at the lesion site as a function of dose, duration of retention, and the effect of time of administration after the injury [19].

2.8 Blood-Spinal Cord Barrier:

Evans Blue (EB) dye extravasation method that we previously developed using Maestro to determine the blood-brain barrier permeability in stroke conditions was explored to determine the blood-spinal cord barrier (BSCB) permeability [24]. The optical imaging method is 1000-fold more sensitive than the spectrophotometric method commonly used to quantify EB dye in tissue. The dye solution (4% w/v in saline, 2.5 ml/kg) was injected intravenously 2 hours before terminating the study at 24 hours post-injury. After cardiac perfusion to wash out the dye from the circulation, spinal cords were isolated and imaged using Maestro. Two sets of images were captured, one with a blue filter and another with a near-infrared (NIR) filter. The blue filter (wavelength 500–720 nm, exposure time 787 ms)

captures an outline and background signal of the spinal cord, while the NIR filter captures (wavelength 740–950 nm, exposure time 1183.04) the dye signal.

2.9 Localization of NPs at Lesion Site:

After cardiac perfusion with saline to wash out the NPs from the circulation, the harvested spinal cords were imaged using Maestro with the blue filter to capture the background image (wavelength 500–720 nm, exposure time 1031.3 ms) and then the NIR filter (wavelength 740–950 nm, exposure time 873.21 ms) to visualize the NIR dye signal in NPs. After un-mixing the spectra of the NIR dye signal from the background signal, the co-localized images of spinal cords are due to the dye signal. The region of interest (ROI) was used for the total signal count to compare the relative localization of NPs. Heat maps illustrate the relative signal intensity due to the localization of NPs in the spinal cord. Following imaging, lesion segments of the spinal cords were homogenized. A standard plot created in control spinal cord tissue homogenate was used to quantitatively determine the total amount of NPs localized at the lesion site [19].

2.10 Determination of ROS Levels:

CellROX deep red reagent (ThermoFisher Scientific, Waltham, MA) was used to measure the relative ROS activity at the lesion site. The assay involves the conversion of a colorless dye into a deep red fluorescence product upon oxidation by ROS and other oxidizing free radicals formed. The assay was performed with and without treatment with antioxidant NPs or enzymes administered 3 hours post-injury, and the spinal cords were analyzed 24 hours post-treatment. To perform the assay, spinal cords were cut into 1 cm segments, which included the lesion site. These segments were incubated with the CellROX reagent (5 μMol/L) in a water bath maintained at 37 °C for 30 minutes, washed with PBS (1X) three times, and immediately imaged using Maestro. The blue filter was set between 500 and 720 nm wavelengths with an exposure time of 800 ms for the background signal. The yellow filter was set at 630–800 nm, with an exposure time of 800 ms, to capture the fluorescence signal of the oxidized dye after its reaction with ROS. The ROI was used to capture the signal, and the signal from the uninjured spinal cord was used as a background signal. The data were computed as the percent of signal change in the spinal cord signal from untreated and treated animals with respect to the control (uninjured) spinal cord segment.

2.11 Processing of Spinal Cords for Immunohistochemical Staining:

Harvested spinal cords were fixated in 4% buffered PFA (Santa Cruz, Dallas, TX) at room temperature for ~48 hours and then placed into 70% ethanol (Pharmco-AAPER, Brookfield, CT) for 24 hours. The spinal cords were trimmed to ~2 cm sections, including the lesion site, and embedded in paraffin. Formalin-fixed paraffin-embedded (FFPE) spinal cords were then cut in 5–10 μm sections on a longitudinal plane with a microtome (Leica RM2135, Buffalo Grove, IL) and mounted onto microscopic slides (Superfrost Plus, Fisher Scientific, Pittsburgh, PA).

2.12 Immunohistochemical Staining:

Spinal cord sections were deparaffinized, rehydrated, and antigen retrieved in 2 steps (30 min each) of steaming Trilogy® (produced by Cell Marque and bought from Sigma-Aldrich). Afterward, the container with Trilogy and slides was allowed to cool down for 5 min on the bench, followed by one rinse with water. The endogenous peroxidase in the tissue sections was then neutralized with 0.3% H_2O_2 (Sigma-Aldrich) in 80% methanol (Pharmco-AAPER, Brookfield, CT) for 20 min at room temperature. After that, the sections were rinsed in PBS, followed by overnight incubation at 4 °C with primary antibodies diluted in antibody diluent with background-reducing components (Agilent Technologies, Santa Clara, CA, item# S3022). Primary antibodies used were: rabbit (Rb) anti-Caspase-3 to detect apoptotic cells (1:200 dilution, R&D Systems, Minneapolis, MN; item# AF835), Rb anti-myeloperoxidase (MPO) to detect neutrophils (diluted 1:50. Abcam, Waltham, MA, item# ab65871*)*, Rb anti-β3-tubulin to detect immature neurons (1:2000 Abcam, Waltham, MA, item# ab18207), and Rb anti-Iba1 to detect microglia (1:500, FUJIFILM Wako Chemicals, Richmond, VA, item# 019–19741). The slides were washed three times with PBS for 5 minutes each, and sections were incubated with HRP labeled Rb SuperPicTure Polymer (ThermoFisher Scientific, Waltham, MA, item# 87–9263) for 10 min at room temperature. This was followed by two washes with PBS for 1 minute each and, after that, HRP substrate DAB (ThermoFisher Scientific, Waltham, MA, item# 87–9999) for up to 10 minutes at room temperature. The sections were rinsed three times in water (1 min each). For slides with β3-tubulin and Iba1staining, cell nuclei were counterstained with Mayer's hematoxylin (Sigma-Aldrich) and rinsed with tap water, followed by a clarifying step with Richard Allen Clarifier 1 (Avantik, Pine Brook, NJ) and the final step with Richard Allen Bluing Reagent (Avantik, Pine Brook, NJ). For slides with Caspase-3 and MPO staining, the cytoplasmic proteins were counterstained with Eosin Y-solution 0.5% alcoholic (Sigma-Aldrich, item# 102439). After nuclear and cytoplasmic counterstaining, respectively, the sections were dehydrated through increasing concentrations of ethanol for 5 min each (50%, 70%, 90%, and 100%) followed by two rinses (5 min each) in Citrus Clearing Solvent (Avantor-VWR, Bridgeport, NJ). Finally, coverslips were mounted over the sections using Richard-Allan Scientific® Mounting Medium (Avantor-VWR). The sections were scanned at 5–20 x magnification with a Leica DM6B upright microscope scanner equipped with a Leica DFC 7000T camera (Leica Microsystems, Wetzlar, Germany).

2.13 Staining for Collagen:

Gomori's Trichrome Stain kit (Sigma-Aldrich) was used to analyze the collagen content at the lesion site of the spinal cords collected at the study endpoint of 4 weeks. Spinal cord sections were deparaffinized in xylene (Avantik, Pine Brook, NJ), rehydrated in decreasing concentrations of alcohol, and rinsed in water. The sections were then placed in Bouin's Fluid (supplied in the kit) overnight at room temperature, followed by counter-staining with hematoxylin (Sigma-Aldrich) and staining with Trichrome stain (provided in the kit). After rinsing with 1% acetic acid (Sigma-Aldrich), the sections were dehydrated in increasing concentrations of alcohol and mounted with Richard-Allan Scientific® Mounting Medium. The mounted sections were allowed to dry, and coverslips were placed over them using the same mounting medium. The sections were then scanned with a Leica DM6B upright microscope scanner.

2.14 Staining for Myelin:

Spinal cords collected at the study endpoint of 4 weeks were used to analyze myelin content. Spinal cord sections were deparaffinized in Xylene, rehydrated in ethanol, and then incubated overnight with Luxol fast blue solution (Sigma-Aldrich) at 56°C. The excess stain was rinsed off the following day with 95% ethanol and then with distilled water. Next, the sections were differentiated in an aqueous lithium carbonate solution (CPLSafety, Novato, CA) for 30 seconds, 70% ethanol for 30 seconds, and then with water. The above three differentiation steps were repeated until a clear difference between the gray and white matter was observed under a microscope. Next, the sections were counterstained with Cresyl violet solution (Sigma-Aldrich) for 30–40 seconds, differentiated in 95% ethanol, and then rinsed in 100% ethanol and xylene. Finally, the slides were rinsed in 100% ethanol twice for 5 min, then in xylene twice for 5 min, and coverslips were mounted over the sections using Richard-Allan Scientific® Mounting Medium. Mounting media was allowed to dry, and the sections were scanned with a Leica DM6B upright microscope scanner.

2.15 Quantification:

For quantification, three randomly selected different areas (3 mm^2) from each section were analyzed using QuPath-0.3.0 (the University of Edinburgh, Edinburgh, Scotland) as per the protocol described elsewhere [25]. In brief, the sections were split into different color channels (Blue, Red, and Green), followed by thresholding to count the positive cells in their respective channels. The above method determined the percentages of microglia, caspase-3 +ve (apoptotic cells), and neutrophil-positive cells. Image Pro 10 (Media Cybernetics, Inc.1700 Rockville, MD) tools were used to quantify collagen and myelin content. For collagen (2 mm^2), epicenter areas were analyzed to quantify the percentage of tissue area containing collagen. Using the same method, myelin was calculated per mm^2 of tissue, and the data were calculated as the percent loss of myelin compared to that in a normal spinal cord.

2.16 Nissl Staining:

After washing in PBS overnight, spinal cord segments were kept in a 15% sucrose solution until they sank. They were then transferred to 30% sucrose and kept overnight at 4 °C until then for embedding in paraffin. The paraffin blocks were sectioned at 10 μm thickness with a Microtome (Leica RM2125, Buffalo Grove, IL), and then the sections were mounted on Superfrost Plus Microscope slides (Fisher Scientific). For Eriochrome Cyanine (EC) staining, the slides were put on a slide warmer at 37°C for 1–2 h, then in fresh 100% acetone for 5–10 min at RT. The slides were stained in freshly filtered EC solution for ~30 min at room temperature, then washed in gently running tap water for 4–5 min. The sections were differentiated in 5% iron alum for 5–15 min at RT. To Complete the differentiation, slides were put in the borax-ferricyanide (Sigma Aldrich) solution at RT for 3–10 min. To counterstain the sections, the slides were placed in 80% alcohol for 3 min, followed by staining in 1% Cresyl Violet solution (Sigma Aldrich) for 7–10 min. The slides were washed in running tap water for a few seconds, dried well, and then placed in 95% alcohol containing 0.1% acetic acid for 5 min. Finally, the slides were placed in 95% alcohol for 2 × 2 min (neuronal cytoplasm light violet, nuclei dark blue), followed by putting in 100%

alcohol for 2 × 5 min to complete dehydration. Coverslips were mounted over the sections and were scanned at 5–20 x magnification with a Leica DM6B upright microscope scanner equipped with a Leica DFC 7000T camera (Leica Microsystems, Wetzlar, Germany).

2.17 Magnetic Resonance Imaging (MRI):

MRI was used to visualize and quantify the lesion volume at the study endpoint four weeks after the injury. Following cardiac perfusion of animals with 4% PFA, harvested spinal columns were imaged using MRI (Bruker Inc., Billerica, MA). They were cut into ~ 4.0 cm in length, including the lesion site in the center, and soaked into ~3.0 mM Gd solution (Cardinal Health, Cardinal Place Dublin) for 7 days. The cranial end of the spinal column was put first into the bore of the MRI and scanned using a horizontal Biospec 9.4T scanner with a 23-mm birdcage coil (Bruker Inc., Billerica, MA). The images obtained were then analyzed using 3D slicer software (3D slicer 4.10.1, Kitware Inc., Clifton Park, NY) to mark the lesion area and quantify the lesion length and volume using the segment statistics tool [26].

2.18 Basso-Beattie-Bresnahan (BBB) Scoring:

Following a single dose intravenous (tail vein) administration of antioxidant NPs (30 mg/kg, equivalent to total enzymes, SOD + CAT = 1.9 mg or 9,500 Units) at 3 hours post-SCI, animals were assessed regularly for the open field locomotion BBB rating scale. Data were collected in a blinded fashion and analyzed after the completion of the study. Control groups were the animals treated with enzymes in solution, saline control, and control NPs. The BBB scale ranges from 0 to 21 and reflects functional recovery after SCI. Scores from 0 to 7 indicate no or minimal hindlimb movement, 8 to 13 indicate intermittent stepping with no or little coordination, and scores from 14 to 21 indicate increasing coordination and functional recovery [9].

2.19 Footfalls:

At the study endpoint at 4 weeks, animals were examined in a custom-made chamber consisting of 32 inches in length and 18 inches in breadth with 3 cm square spaced metal rungs over which animals traversed to move on the surface (Cleveland Clinic, Machine shop). Animals were allowed to move on metal rungs for five minutes. Footfalls were considered when the hind limb failed to grasp a bar and fell between the bars. Ethovision XT (Noldus, Leesburg, VA) video tracking system determined the distance traveled in 5 minutes. The other camera (Cannon, Japan) was set parallel to the grid walk mesh to monitor footfalls. The data were computed as the number of footfalls/inch distance traveled.

2.20 Randall-Selitto Test:

Analgesy-meter was used to assess neuropathic pain response at the study endpoint at 4 weeks. It exerts an increasing force at a constant rate and is continuously monitored by a pointer moving along a linear scale. Each animal was acclimatized to the device and immobilized into a soft cotton cloth to place the hind paw under the cone-shaped pusher with a rounded tip. Next, a force (ranging from 0 to 250 g) was applied to the animal's hind paw, which was placed on a small plinth under the cone-shaped pusher with a rounded

tip. The pedal switch was used to start the test and released when the animal responded to the force, such as paw withdrawal, struggling to withdraw the paw from the tip, or vocal response. A digital meter recorded the data in gram force (gf). The test was performed on each animal with a gap of 30 minutes, and an average of three readings was taken.

2.21 Thermal Sensitivity Evaluation (Hot Plate):

The study endpoint at 4 weeks, sensory stimulation of hind paws was assessed using a preheated (50 °C) plate (IITC Inc. Life Science, CA). The animal's latency to respond to the heat, such as lifting or licking a hind paw, jumping, and/or vocalizing, was recorded with a 20-second cut-off for monitoring the response. The data were calculated in seconds as hind paw latency to the response.

2.22 Statistical Analyses:

The mean and standard error of the mean (s.e.m.) were calculated for the data, and the statistical significance between groups was analyzed using GraphPad Prism software, Version 9 (GraphPad Software Inc., San Diego, CA). Multiple unpaired t-tests with Welch correction were used to statistically analyze BBB scores and weight changes with and without treatment. One-way analysis of variance (ANOVA) or Student's t-tests were used for other comparisons, depending on the number of groups being compared. A p-value of less than 0.05 was considered significant.

3. Results

3.1 Nanoparticle characterization.

The hydrodynamic diameter measured in an aqueous dispersed state, which includes the diameter of NP and the associated water due to hydration, is larger than the TEM diameter, which is measured in a dry form of NPs. Polydispersity index <0.1 indicates uniform particle size distribution. Near-infrared dye-loaded and control NPs have similar physical properties as antioxidant NPs. These NPs have negative zeta potential (Table 1). Also, as determined previously, antioxidant NPs are spherical in shape, and the release of antioxidant enzymes is sustained, with 45% of SOD and ~60% of CAT release occurring in one week [20].

3.2 Blood-spinal cord barrier (BSCB) permeability, NP localization, and ROS levels post-treatment.

The spinal cord images taken 24 hours post-injury show the signal of Evans blue dye, indicating disruption of the BSCB due to contusion injury (Figure 1A). When the dye-loaded NPs are administered intravenously 3- and 6 hours post-injury, the spinal cord images taken 24 hours after their administration show localization of NPs mainly at the lesion site; however, when administered 24 hours post-injury and the image taken 24 hours after administration, localization of NPs in spinal cord is diffused, progressing more towards the cranial to the lesion site than the caudal side of the spinal cord (Figure 1B–a). This could be due to the edema, causing NPs to diffuse through the lesion site along the spinal cord through the gaps between nerve fibers. In addition, edema causes microvascular damage [27]. After the SCI, edema is progressive, reaching a peak during the acute/subacute phase

before reaching the baseline at ~1 week [28]. The cross-sectional images of the spinal cord from the lesion site show NP localization within the lesion cavity, indicating extravasation of NPs from the circulation to the spinal cord tissue through the disrupted BSCB. The uptake of NPs at the lesion area is similar when they are administered at 3- and 6 hours post-injury but is reduced marginally when administered 24 hours after the injury (Figure 1B–b). Using a standard plot created in control spinal cord tissue homogenate, the uptake of NPs at the lesion area is approximately 15 μg. The treatment with antioxidant NPs, administered at 3 hours post-injury, and the lesion site analyzed 24 hours after the treatment show complete neutralization of the post-injury elevated ROS levels, whereas an equivalent dose of antioxidant enzymes administered in solution shows a marginal effect (Figure 1C).

3.3 Early events following injury in treated and untreated groups.

In treated animals, the accumulation of neutrophils and macrophages at the lesion area is significantly reduced, indicating a diminished inflammatory response (Figure 2A). Further histological analysis of the spinal cord at 6 days shows considerably smaller and fewer lesion cavities in treated than in untreated control. Analysis of the spinal cord sections accumulation of microglia in and around the lesion cavity in treated animals, whereas, in untreated animals, they are mainly seen as unorganized clusters near the lesion area and very few within the lesion cavity (Figure 2B).

3.4 Chronic events after treatment with antioxidant NPs:

Visual examination of the harvested spinal cords at 4 weeks shows a smaller lesion area (marked dark grey area) in treated than in untreated animals (Figure 3A–a). This observation is further supported by histological analysis of the spinal cord sections, which, in treated animals, shows significantly reduced cavitation and signs of healing of the lesion cavity, whereas, in untreated animals, these cavities are larger with no indication of healing (Figure 3A–b). Further analysis shows that the collagen content in the lesion cavity of the treated animals is significantly lower than that of the untreated animals (Figure 3B). In addition, the treatment attenuates the post-injury demyelination of axons (Figure 3C). The high-magnification images display the continuous nature of the myelinated nerve fibers in treated animals, whereas these are unorganized, with vacuoles, and discontinuous in control (Figure 3C, enlarged images). A significantly reduced number of apoptotic cells are seen in the spinal cord sections of treated than untreated animals (Figure 3D). Apart from the area around the lesion site, in serial spinal cord sections, the number of apoptotic cells in the caudal to the lesion site is greater in untreated versus treated animals (Figure 3E).

3.5 Syringomyelia, cellular events, and lesion cavity.

Spinal cord analysis at 4 weeks post-injury shows the formation of syringomyelias – the fluid-filled cysts (syrinx); these are seen in about 75% of untreated animals but not in treated animals (Figure 4A). Syringomyelias cause swelling of spinal cords because of fluid accumulation, which is also evident from these images (Figure 4A). Further analysis of the spinal cord sections at 4 weeks indicates the presence of amoeboid-shaped microglia in untreated animals, whereas they are rod-shaped in treated animals (Figure 4A, enlarged images). A significantly higher number of activated microglia are seen in treated animals, even distal to the lesion site, but not in untreated animals; their numbers are very close to

that in naïve control (Figure 4B, graph). Enlarged images of these sections show differences in the morphology of microglia; they appear more ramified (as expected) in the spinal cord sections of a normal (uninjured) animal, are ameboid-shaped in injured and untreated animals, and are rod-shaped and ramified in injured and treated animals (Figure 4C). When the sections are analyzed for immature neurons, their number is greater at the lesion site in treated versus untreated animals (Figure 4D).

MRI of the isolated spinal cords taken at 4 weeks shows a 2.5-fold reduction in lesion volume in treated versus untreated animals (Figure 5A, C). The lesion length determined from the serial cross-sectional images when the grey matter structure is visible from the cranial to caudal end is significantly smaller for the treated vs. untreated animals (6.8 ± 0.7 mm vs. 14.9 ± 1.6 mm; mean ± s.e.m., n=3, **<0.001) (Figure 5B). The close observation of these sections, particularly in the epicenter region, shows the presence of grey matter in treated animals but not in untreated animals (Figure 5B). Histological analysis of the spinal tissue sections using Nissl staining further confirms the above assessment of the treatment effect (Figure 5D).

3.6 Functional recovery.

Treated animals demonstrate a steady improvement in the BBB scores over 4 weeks, whereas untreated and other controls (enzymes in solution or control NPs without antioxidant enzymes) animals show the BBB scores reaching a plateau in ~2 weeks (Figure 6A–a). The increase in the BBB scores from the initial time point post-injury is by ~ 4–6 points in untreated and control animals, whereas this increase is by ~12 points in antioxidant NPs treated animals compared to control NPs (Figure 6 A–a). The endpoint BBB score at 4 weeks of ~17 in treated animals signifies forelimb and hindlimb coordination, whereas a score of 5–9 in untreated and other control groups reflects isolated joint movements with little or no hindlimb movement or rare intervals of uncoordinated stepping. Treated animals also show less weight loss at 1 week than untreated (3–4% vs. 8–9%), and they regain weight to the pre-injury level in 3 weeks, whereas untreated animals remain below the pre-injury level by ~4 % until the study endpoint at 4 weeks (Figure 6A–b).

The above data analysis based on the sex of animals shows no significant differences in the BBB scores. However, weight gain by male and female rats is much faster in treated animals than in untreated animals. Comparing the male and female weight data in untreated groups, male rats gain weight better, whereas female rats fail to recover from the post-injury weight loss (see supplemental section). It is to be noted that this study was not designed and powered to test the differences between the sexes, but it is an important biological variable in SCI that requires further investigation [29].

The grid walk test shows that treated animals have fewer footfalls than untreated animals (Figure 6 B–a). The distance traveled by treated animals is also greater than that of untreated animals, although the difference is not statistically significant (Figure 6 B–b). Evaluation of the animals' pain resulting from the Randall-Selitto probe at 4 weeks shows a higher paw withdrawal threshold for the treated animals than untreated animals (Figure 6 C–a). The analysis of thermal hyperalgesia (hot plate) at 4 weeks shows a 24% reduction in the sensory

threshold in untreated animals, while for treated animals, the reduction is 13 % compared to the pre-injury level (Figure 6 C–b).

4. Discussion

Despite ongoing research into regenerative therapies (e.g., scaffold, neuroprotective agents, stem cells, growth factors) and approaches like electrical stimulation and intensive rehabilitation strategies for chronic SCI, their effectiveness in achieving neurological and functional recovery remains limited [30]. After chronic SCI, intrinsic factors such as the low regenerative ability of neuronal cells and inhibitory factors in the spinal cord microenvironment limit the regenerative capacity of axons, and the scar tissue formation at the lesion site impedes their connectivity [31]. As a result, there are concurrent efforts in developing early interventions to protect the injured spinal cord from secondary injury progression in anticipation that it will lead to improved long-term recovery [32].

The secondary injury cascade encompasses a dynamic series of complex cellular and molecular events [27]. These changes involve vascular disruption, edema, excitotoxicity, inflammation, oxidative stress, and apoptosis, collectively leading to progressive degeneration of the injured spinal cord [33]. In this study, we targeted the excessive ROS formed at the lesion site as the key mediator of the cascade of degeneration, triggering a vicious cycle of secondary injury progression [34]. Under normal circumstances, ROS or free radicals generated as a part of normal metabolic activities are effectively and instantly neutralized by the endogenous antioxidant defense mechanism, which includes antioxidant enzymes within cells and tissues. This mechanism maintains the crucial redox balance for normal cellular functioning; however, following neural tissue injuries like spinal cord or brain injuries, this redox balance is disrupted as the endogenous antioxidant defense mechanism becomes inadequate to counteract the excessive production of ROS. Further, the genes responsible for encoding antioxidant enzymes are downregulated after the injury [35]. Neural tissues are particularly vulnerable to ROS-induced damage due to their high content of unsaturated fatty acids and low antioxidant capacity [33].

Our data demonstrate that treatment with antioxidant NPs significantly mitigates the secondary injury progression, including protecting the spinal cord tissue from apoptosis (Figure 3). In addition to the vicinity of the lesion site (Figure 3D), apoptosis was also seen caudal to the lesion in untreated animals (Figure 3E), which could affect bladder, bowel, sexual, and muscle functions [36]. The treatment inhibited syringomyelia formation, but in untreated control, they are seen expanding from the lesion site towards the cranial side, which could affect respiratory and cardiac functions [36] (Figure 4). After SCI, overall body physiology changes due to disruption in the neural circuitry and signals to vital organs, and this continues to aggravate because of the progressive degeneration of the spinal cord tissue [1]. The treatment with antioxidant NPs exhibited favorable effects on the factors that hinder axonal connectivity and signal conduction, such as reduced cavitation (Figure 3A), scar-forming collagen at the lesion site (Figure 3B), and restricting the expansion of lesion size (Figure 5). Additionally, axons are protected from demyelination, which is crucial for efficient neural signal conduction (Figure 3C) [37]. Importantly, immature neurons in the lesion cavity in treated animals indicate the regenerative process (Figure 4D).

In our previous study, we investigated the effect of antioxidant NPs on mitochondrial characteristics, where the treatment was administered 6 hours after the injury, and the spinal cords were analyzed one week after treatment. The results demonstrated attenuation of post-injury mitochondrial dysfunction, providing the necessary energy (ATP) to help restore cellular and metabolic functions [20]. Moreover, the mitochondria isolated from the lesion site of the treated animals showed reduced mitochondrial ROS levels, improved mitochondrial membrane potential, and decreased calcium levels. Immunohistochemical analyses of the spinal cord tissue from the treated animals further confirmed significantly reduced ROS, cleaved caspase-3, and cytochrome c activities. This resulted in the spinal cord tissue protection from apoptosis [20]. These findings are significant, as dysfunctional mitochondria are a major source of ROS formation and contribute to the degeneration of axons [7].

A consistent improvement in the BBB scores was observed over time in treated animals, indicating an enhanced motor function recovery (Figure 6A–a). The treatment also improved sensory perceptions, as demonstrated by a reduced number of footfalls in the grid walk test (Figure 6B–a,b) and an increased threshold for pain and heat perception (Figure 6C–a,b). Furthermore, the treated animals exhibited a faster weight regain than untreated animals, suggesting improved health status (Figure 6A–b). These findings collectively demonstrate the beneficial effects of the treatment on multiple functional aspects and overall well-being.

The therapeutic efficacy of antioxidant NPs can be attributed to multiple factors, with the catalytic mechanism of action of the encapsulated antioxidant enzymes being particularly significant. These enzymes played a critical role in neutralizing the excessive ROS formation at the lesion site, even with a relatively small dose of approximately 11–15 μg antioxidant NPs localized at the lesion site (or 125 mg spinal cord tissue taken for analysis), equivalent to ~ 4,000 milliunits of SOD and CAT at the lesion site (32 Units/g spinal cord tissue) or ~660 ng at the lesion site (5.3 μg/g spinal cord tissue) (Figure 1). In normal rat spinal cord tissue, the SOD level is ~ 1.4 U/g tissue, whereas the CAT level is ~2 U/g tissue [38]. In human cerebrospinal fluid, CAT level is 2.2 ± 0.6 mU/ml and SOD is 0.17 ± 0.1 U/ml [39]. These values reflect the high potency of antioxidant enzymes to maintain the redox balance under normal conditions. Since we show complete neutralization of excess ROS, the low dose of antioxidant enzymes delivered to the lesion site using antioxidant NPs is effective in regaining the redox balance. The extravasation of intravenously injected NPs from the circulation to the lesion site through the permeable BSCB is also crucial for their effectiveness (Figure 1). The depot effect of the NPs localized at the lesion site [19] provides their long-term antioxidant effects, protecting the spinal cord from the continued oxidative stress-induced damage [14]. Diffusion of antioxidant NPs through the spinal cord could have protected the ischemic penumbra from ischemia-reperfusion injury, an event occurring after the SCI (Figure 1C).

Only a few studies assessed the use of antioxidant enzymes via intravenous administration for acute SCI, such as polymer-SOD1 complex [40] and PEP-1–SOD1 fusion protein [41]. These were administered at 30 min or immediately after the injury, and functional recovery was minimal. For example, multiple dosing of PEP-1–SOD1 improved BBB score by 2 points at 35 days. In that regard, our results are significantly better considering that the

treatment was administered 3 hours post-injury, and improvement in the BBB scores is higher with our treatment than reported in the above studies. Since the BSCB remains permeable to the intravenously administered NPs even at 24 hours post-injury (Figure 1), there is potential to evaluate the treatment efficacy beyond the 3-hour treatment window evaluated in this study. Despite the persistence of ROS for at least up to 10 days post-injury [42], determining the optimal treatment time window is crucial to assess the potential benefits of delayed intervention with antioxidant NPs, considering that the factors beyond ROS may become inhibitory with time [43]. It is reasonable to anticipate that the treatment window in humans could be longer than that optimized in rat models because of a significant difference in basal metabolic rates between rats (6.4 times higher) and humans [44].

The synergistic effect of SOD and CAT is crucial for efficiently detoxifying ROS at the lesion site. Dismutation of superoxide anion (O_2 •−) by SOD produces hydrogen peroxide (H_2O_2), which has a damaging effect on cells and tissue, but CAT neutralizes it to form inert oxygen and water [45]. Superoxide anion (O_2 •−), as such, is not considered a potent oxidizing agent, but it triggers the formation of a variety of ROS, reactive nitrogen species (RNS), and peroxynitrite (ONOO−), from which many additional secondary radical species are generated. By controlling superoxide anion (O_2 •−), SOD controls the formation of all these reactive species [46]. The SOD-catalyzed dismutation reaction is highly efficient in detoxifying ROS. In addition, SOD has an anti-inflammatory effect as it can remove the activated neutrophils by apoptosis, thus controlling neutrophil-mediated tissue injury [47]. Our data show fewer neutrophils in the spinal cord section of treated animals than in untreated animals (Figure 2A). Excessive H_2O_2 is a deleterious oxidant that damages cell membrane proteins and interacts with soluble Fe(II) iron, known as Fenton’s reaction, producing hydroxyl radicals that cause DNA damage. In addition, certain amino acids (e.g., L-histidine, L-cystine) and other cellular components can boost the toxicity of H_2O_2 [48]. For these reasons, we used a combination of SOD and CAT in antioxidant NPs.

Although only a small fraction (~0.2% efficacy) of intravenously injected antioxidant NPs localize at the lesion site, the biodistribution of these NPs throughout the body is considered safe due to the endogenous nature of the encapsulated antioxidant enzymes and the use of FDA-approved biodegradable and biocompatible polymer, PLGA. Previously, we determined the biocompatibility of antioxidant NPs in neurons in vitro [18] and in zebrafish [49], and recently in mice with PLGA-based NPs, which did not show any significant changes in tissue/blood inflammatory cytokine levels or vital organ tissues following histological analysis [50]. This distinguishes antioxidant NPs from other drugs like steroids or anti-inflammatory drugs, where toxicity is a concern, particularly in SCI patients due to altered physiology and its implications on drug pharmacokinetics and metabolism [51]. The biodistributed dose of antioxidant NPs likely protects vital organs and other tissue from increased systemic levels of ROS and inflammatory cytokines triggered by SCI [2]. Significant evidence of oxidative stress-induced DNA damage in vital organs, including the brain, indicates systemic genotoxicity in patients with SCI [52]. The observation that treated animals show better weight gain than untreated animals (Figure 6A–b) suggests that antioxidant NPs, in addition to protecting the spinal cord, may also confer protection to other organs. Direct intraspinal or intrathecal injection of antioxidant NPs could be effective at lower doses than intravenous administration. However, this approach requires specific

resources and expertise, potentially causing a delay in treatment initiation. Nevertheless, it remains an option to explore in certain situations.

Syringomyelias are the development of fluid-filled cavities (syringes) along the central canal and tethered spinal cord, extending towards the cranial direction [31] (Figure 4A). Their formation results in swelling of the spinal cord and obstruction in the flow of the cerebrospinal fluid [53]. In general, syringomyelia formation has devastating effects, causing new levels of disability, particularly respiratory failure. These effects can occur long after the initial injury and even after a successful rehabilitation, indicating the impact of secondary injury continues over a prolonged period [54]. Investigating the effects of antioxidant NP treatment on the permeability of the BSCB and edema would be of great interest, as both events are considered detrimental to secondary injury progression [55].

Clearing the dead tissue is the first step in the body's repair mechanism. In response to the injury, macrophages are recruited from the circulation to the lesion site, and endogenous activated microglia can clear the dead tissue. In our study, we see the presence of large cavities in the spinal cord sections of injured untreated animals, which could be due to impaired clearing of dead cell debris [56]. It has been reported that circulating macrophages become dysfunctional under oxidative stress conditions [57], which may explain the presence of large cavities in the spinal cord sections of untreated animals (Figures 4A and 5). These cavities were very few and smaller in treated animals, indicating that by mitigating oxidative stress, macrophages/activated microglia were able to scavenge cell debris (Figure 2). Additionally, in treated animals, activated microglia are seen in and around the lesion cavity at 6 days, forming a "microglia plug" which may contribute to containing the lesion site and protecting the spinal cord from circulating inflammatory cells and proteins [58] (Figure 2B).

Although we did not study astrocytes, beginning at 1–2 days after injury, they are reported to densely populate the area around the lesion core and, within a 7–10-day period, lead to glial scar formation, which is characterized by the deposition of inhibitory chondroitin sulfate proteoglycans. The glial scar plays a dual role in SCI, both protective by restricting the spread of inflammation and inhibitory by acting as a barrier to inhibit axonal regrowth [59]. Since we see reduced collagen deposition in the lesion site but rather the formation of immature neurons in treated animals (Figure 3), it is less likely that astrocytes are promoting glial scar tissue formation, which could be the effect of the treatment, neutralizing ROS. Nonetheless, further investigation is needed to streamline the role of different cells in protecting the spinal cord following treatment with antioxidant NPs.

At 4 weeks, the spinal cord sections and MRI analysis show the presence of large cavities and greater lesion length and volume in untreated animals than in treated animals (Figures 3–5). Depending upon the environment they are exposed to, activated microglia could play contradicting roles, from protective to degenerative [60]. Under oxidative stress conditions, microglia lose their healing ability [61] and become more pro-inflammatory [62]. Interestingly, in our study, immunohistochemical analysis of the spinal cord sections from untreated animals shows more amoeboid-type microglia, whereas the sections of treated animals show more rod-shaped microglia (Figure 4A). Rod-shaped microglia are

neither an M1 nor an M2 phenotype, but under adverse conditions such as oxidative stress, they can rapidly transform into an amoeboid form and become M1-activated [63]. M1 microglia release inflammatory mediators and induce inflammation and neurotoxicity, while M2 microglia release anti-inflammatory mediators and induce anti-inflammatory and neuroprotectivity [64]. It is interesting to note that the number of microglia in untreated animals is the same as in naïve control (uninjured), but they are significantly higher in treated animals even at 4 weeks (Figure 4B, graph). The oxidative stress condition in untreated animals could potentially be affecting their activation and mobility toward the lesion site to facilitate the regenerative process.

While microglia-driven neuroinflammation has a beneficial effect on scavenging cell debris, tissue healing, and repair, it is also becoming apparent that their chronic activation leads to the noxious impacts on neurons and, thus, participates in the pathophysiology of neurodegenerative diseases [65]. The ROS produced by the surrounding environment can modulate microglial activity and could become disease-associated microglia, contributing to disease progression [66]. Although systematic studies are needed to characterize microglia and understand their transformation following treatment with antioxidant NPs, activated rod-shaped microglia in treated animals could have favorably protected the injured spinal cord, promoting a regenerative process. In contrast, amoeboid microglia in untreated animals could have triggered pro-inflammatory and degenerative effects, further expanding the lesion site.

As demonstrated in our previous study in a rat thrombolytic stroke model, the addition of antioxidant NPs to standard anti-thrombolytic treatment promoted the migration of stem cells from the subventricular zone and circulating progenitor cells to the lesion site and differentiation into neural cells– a result not seen in the animals untreated or treated with only thrombolytic agent [67]. A similar repair mechanism could also be activated in SCI following treatment with antioxidant NPs. Prior studies by others have demonstrated that following spinal cord injury, neuronal progenitor cells in the ependymal layer of the spinal cord are activated and undergo migration. During migration, neuronal progenitor cells differentiate from immature to mature neurons. However, this process is influenced by the surrounding environment and can be inhibited by conditions of oxidative stress and inflammation [68]. The treatment with antioxidant NPs, by regaining the redox balance and mitigating inflammation, could favor such migration of progenitor cells and their differentiation in neuronal cells. The immune-histological analysis shows that many cells in the lesion site of treated animals express β3-tubulin (Figure 4D), a marker for immature neurons, indicating neuronal regeneration.

Our data show reduced collagen formation at the lesion site in the treated group compared to the untreated control. The ROS have been implicated in promoting fibrosis (collagen deposition) [69] and hinder axonal regeneration and connectivity across the lesion cavity, ultimately affecting the functional recovery [70, 71] (Figure 3B). A critical observation also was reduced demyelination of neurons in treated vs. untreated animals (Figure 3C); myelin plays a crucial role in conducting nerve impulses through the axons [72]. Overall, by neutralizing the excessive ROS and restoring the redox balance at the lesion site, the

treatment could have changed the dynamics in the spinal cord microenvironment from degenerative to protective and regenerative processes (Figure 7).

Methylprednisolone, an anti-inflammatory drug, was used previously for acute post-injury SCI, but clinical outcomes have been inconsistent; instead, it did not demonstrate any enhancement in neurological recovery [73]. In addition, the recent metadata analysis shows that required high doses of it caused severe side effects; hence, it is not recommended [74]. Earlier use of neurotropic factors or other therapeutics for SCI have failed to affect the pathophysiology of secondary injury cascades, primarily because of their short half-lives, poor pharmacodynamics of distribution to the lesion site, and transient retention [75]. Similar issues have been reported for non-catalytic antioxidants when tested for SCI [10]. In this regard, our antioxidant NPs meet multiple treatment objectives – from the delivery of potent catalytic antioxidant enzymes to the lesion site to their role in protecting the spinal cord from oxidative stress and degeneration and promoting regenerative events, ultimately leading to improved functional recovery.

5. CONCLUSIONS

The findings of this study highlight the potential of antioxidant NPs in stabilizing the spinal cord during the acute phase of SCI and facilitating functional recovery. Overall, the results substantiate the role of excessive formation of ROS at the lesion site in triggering the cascade of secondary injury progression. While further research is needed to fully elucidate the cellular and molecular mechanisms involved in the injured spinal cord microenvironment following treatment with antioxidant NPs, the results underscore the significance of restoring redox balance in mitigating the effects of secondary injury progression. Notably, the transformation of activated microglia into rod-shaped anti-inflammatory and regenerative phenotype in treated animals appears to play a crucial role in protecting the injured spinal cord and promoting regeneration. Our data support the notion that long-term recovery following SCI depends on effectively managing the early events after the injury. In summary, antioxidant NPs can be developed as an early therapeutic intervention to stabilize the injured spinal cord for clinical translation.

Supplementary Material

Refer to Web version on PubMed Central for supplementary material.

Acknowledgment:

This work was supported by the National Institute of Neurological Disorders and Stroke of the National Institutes of Health under Grant R01NS092033 and the Department of Defense through the Spinal Cord Injury Research Program under Award No. W81XWH-16-1-0786. Opinions, interpretations, conclusions, and recommendations are those of the authors and are not necessarily endorsed by the Department of Defense. The Schematic for TOC was created using BioRender.com

Abbreviations

Antioxidant NPs	Nanoparticles encapsulating SOD and CAT
ATP	Adenosine 5′-triphosphate

BSA	Bovine Serum Albumin
BSCB	Blood-Spinal Cord Barrier
CAT	Catalase
EB	Evans Blue
F	Female
FFPE	Formalin Fixed Paraffin Embedded
HRP	Horseradish Peroxidase
IV	Intravenously
M	Male
min	Minutes
MPO	Myeloperoxidase
MRI	Magnetic Resonance Imaging
ms	Milliseconds
NIR	Near-Infrared
NPs	Nanoparticles
PBS	Phosphate-buffered saline
PEG	Poly Ethylene Glycol
PFA	Paraformaldehyde
PLGA	Poly (D,L-lactide-co-glycolide)
PVA	Poly (vinyl alcohol)
Rb	Rabbit
ROS	Reactive Oxygen Species
SCI	Spinal Cord Injury
SOD	Superoxide Dismutase

References

[1]. Ahuja CS, Wilson JR, Nori S, Kotter MRN, Druschel C, Curt A, Fehlings MG, Traumatic spinal cord injury, Nat Rev Dis Primers, 3 (2017) 17018. [PubMed: 28447605]

[2]. Ahuja CS, Nori S, Tetreault L, Wilson J, Kwon B, Harrop J, Choi D, Fehlings MG, Traumatic Spinal Cord Injury-Repair and Regeneration, Neurosurgery, 80 (2017) S9–s22. [PubMed: 28350947]

[3]. Mugesh Kanna R, Prasad Shetty A, Rajasekaran S, Timing of intervention for spinal injury in patients with polytrauma, J Clin Orthop Trauma, 12 (2021) 96–100. [PubMed: 33716434]

[4]. Oyinbo CA, Secondary injury mechanisms in traumatic spinal cord injury: a nugget of this multiply cascade, Acta Neurobiol Exp (Wars), 71 (2011) 281–299. [PubMed: 21731081]

[5]. Emerit J, Edeas M, Bricaire F, Neurodegenerative diseases and oxidative stress, Biomedicine and Pharmacotherapy, 58 (2004) 39–46. [PubMed: 14739060]

[6]. Emery E, Aldana P, Bunge MB, Puckett W, Srinivasan A, Keane RW, Bethea J, Levi AD, Apoptosis after traumatic human spinal cord injury, Journal of Neurosurgery, 89 (1998) 911–920. [PubMed: 9833815]

[7]. Wang B, Huang M, Shang D, Yan X, Zhao B, Zhang X, Mitochondrial Behavior in Axon Degeneration and Regeneration, Front Aging Neurosci, 13 (2021) 650038. [PubMed: 33762926]

[8]. Hall ED, Braughler JM, McCall JM, Antioxidant effects in brain and spinal cord injury, J Neurotrauma, 9 Suppl 1 (1992) S165–172. [PubMed: 1588607]

[9]. Fraunberger EA, Scola G, Laliberté VL, Duong A, Andreazza AC, Redox Modulations, Antioxidants, and Neuropsychiatric Disorders, Oxid Med Cell Longev, 2016 (2016) 4729192. [PubMed: 26640614]

[10]. Ashok A, Andrabi SS, Mansoor S, Kuang Y, Kwon BK, Labhasetwar V, Antioxidant therapy in oxidative stress-induced neurodegen-erative diseases: Role of nanoparticle-based drug delivery sys-tems in clinical translation, Antioxidants, In revision (2022).

[11]. Miller ER 3rd, Pastor-Barriuso R, Dalal D, Riemersma RA, Appel LJ, Guallar E, Meta-analysis: high-dosage vitamin E supplementation may increase all-cause mortality, Ann Intern Med, 142 (2005) 37–46. [PubMed: 15537682]

[12]. He L, He T, Farrar S, Ji L, Liu T, Ma X, Antioxidants Maintain Cellular Redox Homeostasis by Elimination of Reactive Oxygen Species, Cell Physiol Biochem, 44 (2017) 532–553. [PubMed: 29145191]

[13]. Uematsu T, Nagashima S, Umemura K, Kanamaru M, Nakashima M, Pharmacokinetics and safety of intravenous recombinant human superoxide dismutase (NK341) in healthy subjects, Int J Clin Pharmacol Ther, 32 (1994) 638–641. [PubMed: 7881700]

[14]. Warner DS, Sheng H, Batinic-Haberle I, Oxidants, antioxidants and the ischemic brain, Journal of Experimental Biology, 207 (2004) 3221–3231. [PubMed: 15299043]

[15]. Tsubokawa T, Jadhav V, Solaroglu I, Shiokawa Y, Konishi Y, Zhang JH, Lecithinized superoxide dismutase improves outcomes and attenuates focal cerebral ischemic injury via antiapoptotic mechanisms in rats, Stroke, 38 (2007) 1057–1062. [PubMed: 17272760]

[16]. Reddy MK, Wu L, Kou W, Ghorpade A, Labhasetwar V, Superoxide dismutase-loaded PLGA nanoparticles protect cultured human neurons under oxidative stress, Appl Biochem Biotechnol, 151 (2008) 565–577. [PubMed: 18509606]

[17]. Reddy MK, Labhasetwar V, Nanoparticle-mediated delivery of superoxide dismutase to the brain: an effective strategy to reduce ischemia-reperfusion injury, FASEB J, 23 (2009) 1384–1395. [PubMed: 19124559]

[18]. Singhal A, Morris VB, Labhasetwar V, Ghorpade A, Nanoparticle-mediated catalase delivery protects human neurons from oxidative stress, Cell Death Dis, 4 (2013) e903. [PubMed: 24201802]

[19]. Gao Y, Vijayaraghavalu S, Stees M, Kwon BK, Labhasetwar V, Evaluating accessibility of intravenously administered nanoparticles at the lesion site in rat and pig contusion models of spinal cord injury, J Control Release, 302 (2019) 160–168. [PubMed: 30930216]

[20]. Andrabi SS, Yang J, Gao Y, Kuang Y, Labhasetwar V, Nanoparticles with antioxidant enzymes protect injured spinal cord from neuronal cell apoptosis by attenuating mitochondrial dysfunction, J Control Release, 317 (2020) 300–311. [PubMed: 31805339]

[21]. Kjell J, Olson L, Rat models of spinal cord injury: from pathology to potential therapies, Dis Model Mech, 9 (2016) 1125–1137. [PubMed: 27736748]

[22]. Metz GA, Curt A, van de Meent H, Klusman I, Schwab ME, Dietz V, Validation of the weight-drop contusion model in rats: a comparative study of human spinal cord injury, J Neurotrauma, 17 (2000) 1–17. [PubMed: 10674754]

[23]. Adjei IM, Peetla C, Labhasetwar V, Heterogeneity in nanoparticles influences biodistribution and targeting, Nanomedicine (Lond), 9 (2014) 267–278. [PubMed: 23799984]

[24]. Jaffer H, Adjei IM, Labhasetwar V, Optical imaging to map blood-brain barrier leakage, Sci Rep, 3 (2013) 3117. [PubMed: 24178124]

[25]. Bankhead P, Loughrey MB, Fernandez JA, Dombrowski Y, McArt DG, Dunne PD, McQuaid S, Gray RT, Murray LJ, Coleman HG, James JA, Salto-Tellez M, Hamilton PW, QuPath: Open source software for digital pathology image analysis, Sci Rep, 7 (2017) 16878. [PubMed: 29203879]

[26]. Noristani HN, Boukhaddaoui H, Saint-Martin G, Auzer P, Sidiboulenouar R, Lonjon N, Alibert E, Tricaud N, Goze-Bac C, Coillot C, Perrin FE, A Combination of Ex vivo Diffusion MRI and Multiphoton to Study Microglia/Monocytes Alterations after Spinal Cord Injury, Front Aging Neurosci, 9 (2017) 230. [PubMed: 28769787]

[27]. Hellenbrand DJ, Quinn CM, Piper ZJ, Morehouse CN, Fixel JA, Hanna AS, Inflammation after spinal cord injury: a review of the critical timeline of signaling cues and cellular infiltration, J Neuroinflammation, 18 (2021) 284. [PubMed: 34876174]

[28]. Seblani M, Decherchi P, Brezun JM, Edema after CNS Trauma: A Focus on Spinal Cord Injury, Int J Mol Sci, 24 (2023).

[29]. Osimanjiang W, Allgood JE, Van Sandt RL, Burns DT, Bushman JS, Sexual Dimorphism in Lesion Size and Sensorimotor Responses Following Spinal Cord Injury, Front Neurol, 13 (2022) 925797. [PubMed: 36994113]

[30]. Hachem LD, Ahuja CS, Fehlings MG, Assessment and management of acute spinal cord injury: From point of injury to rehabilitation, J Spinal Cord Med, 40 (2017) 665–675. [PubMed: 28571527]

[31]. Brodbelt A, Stoodley M, Post-traumatic syringomyelia: a review, Journal of clinical neuroscience, 10 (2003) 401–408. [PubMed: 12852875]

[32]. Torregrossa F, Salli M, Grasso G, Emerging Therapeutic Strategies for Traumatic Spinal Cord Injury, World Neurosurg, 140 (2020) 591–601. [PubMed: 32797989]

[33]. Anjum A, Yazid MD, Fauzi Daud M, Idris J, Ng AMH, Selvi Naicker A, Ismail OHR, Athi Kumar RK, Lokanathan Y, Spinal Cord Injury: Pathophysiology, Multimolecular Interactions, and Underlying Recovery Mechanisms, Int J Mol Sci, 21 (2020).

[34]. Hall ED, Antioxidant therapies for acute spinal cord injury, Neurotherapeutics, 8 (2011) 152–167. [PubMed: 21424941]

[35]. Jia Z, Zhu H, Li J, Wang X, Misra H, Li Y, Oxidative stress in spinal cord injury and antioxidant-based intervention, Spinal Cord, 50 (2012) 264–274. [PubMed: 21987065]

[36]. Hou S, Rabchevsky AG, Autonomic consequences of spinal cord injury, Compr Physiol, 4 (2014) 1419–1453. [PubMed: 25428850]

[37]. Mekhail M, Almazan G, Tabrizian M, Oligodendrocyte-protection and remyelination post-spinal cord injuries: a review, Progress in Neurobiology, 96 (2012) 322–339. [PubMed: 22307058]

[38]. Kazanci B, Ozdogan S, Kahveci R, Gokce EC, Yigitkanli K, Gokce A, Erdogan B, Neuroprotective Effects of Pregabalin Against Spinal Cord Ischemia-Reperfusion Injury in Rats, Turk Neurosurg, 27 (2017) 952–961. [PubMed: 27476927]

[39]. Martin-de-Pablos A, Córdoba-Fernández A, Fernández-Espejo E, Analysis of neurotrophic and antioxidant factors related to midbrain dopamine neuronal loss and brain inflammation in the cerebrospinal fluid of the elderly, Exp Gerontol, 110 (2018) 54–60. [PubMed: 29775745]

[40]. Nukolova NV, Aleksashkin AD, Abakumova TO, Morozova AY, Gubskiy IL, Kirzhanova capital Ie CAC, Abakumov MA, Chekhonin VP, Klyachko NL, Kabanov AV, Multilayer polyion complex nanoformulations of superoxide dismutase 1 for acute spinal cord injury, J Control Release, 270 (2018) 226–236. [PubMed: 29196042]

[41]. Yune TY, Lee JY, Jiang MH, Kim DW, Choi SY, Oh TH, Systemic administration of PEP-1-SOD1 fusion protein improves functional recovery by inhibition of neuronal cell death after spinal cord injury, Free Radic Biol Med, 45 (2008) 1190–1200. [PubMed: 18722523]

[42]. Scheijen EEM, Hendrix S, Wilson DM, Oxidative DNA Damage in the Pathophysiology of Spinal Cord Injury: Seems Obvious, but Where Is the Evidence?, Antioxidants, 11 (2022) 1728. [PubMed: 36139802]

[43]. Fan B, Wei Z, Yao X, Shi G, Cheng X, Zhou X, Zhou H, Ning G, Kong X, Feng S, Microenvironment Imbalance of Spinal Cord Injury, Cell Transplant, 27 (2018) 853–866. [PubMed: 29871522]

[44]. Agoston DV, How to Translate Time? The Temporal Aspect of Human and Rodent Biology, Front Neurol, 8 (2017) 92. [PubMed: 28367138]

[45]. Li R, Zhou X, Liu D, Feng W, Enhancing the activity and stability of Mn-superoxide dismutase by one-by-one ligation to catalase, Free Radic Biol Med, 129 (2018) 138–145. [PubMed: 30227270]

[46]. Wang Y, Branicky R, Noë A, Hekimi S, Superoxide dismutases: Dual roles in controlling ROS damage and regulating ROS signaling, J Cell Biol, 217 (2018) 1915–1928. [PubMed: 29669742]

[47]. Yasui K, Baba A, Therapeutic potential of superoxide dismutase (SOD) for resolution of inflammation, Inflamm Res, 55 (2006) 359–363. [PubMed: 17122956]

[48]. Mahaseth T, Kuzminov A, Potentiation of hydrogen peroxide toxicity: From catalase inhibition to stable DNA-iron complexes, Mutat Res Rev Mutat Res, 773 (2017) 274–281. [PubMed: 28927535]

[49]. Kim MS, Stees M, Karuturi BVK, Vijayaraghavalu S, Peterson RE, Madsen GL, Labhasetwar V, Pro-NP protect against TiO2 nanoparticle-induced phototoxicity in zebrafish model: exploring potential application for skin care, Drug Deliv Transl Res, 7 (2017) 372–382. [PubMed: 28299721]

[50]. Rahman MT, Kaung Y, Shannon L, Androjna C, Sharifi N, Labhasetwar V, Nanoparticle-mediated synergistic drug combination for treating bone metastasis, J Control Release, 357 (2023) 498–510. [PubMed: 37059400]

[51]. Mestre H, Alkon T, Salazar S, Ibarra A, Spinal cord injury sequelae alter drug pharmacokinetics: an overview, Spinal Cord, 49 (2011) 955–960. [PubMed: 21625241]

[52]. Medalha CC, Polesel FS, da Silva VH, Martins RA, Pozzi R, Ribeiro DA, Acute spinal cord injury induces genetic damage in multiple organs of rats, Cell Mol Neurobiol, 32 (2012) 949–952. [PubMed: 22476955]

[53]. Austin JW, Afshar M, Fehlings MG, The Relationship between Localized Subarachnoid Inflammation and Parenchymal Pathophysiology after Spinal Cord Injury, Journal of Neurotrauma, 29 (2012) 1838–1849. [PubMed: 22655536]

[54]. Carroll AM, Brackenridge P, Post-traumatic syringomyelia: a review of the cases presenting in a regional spinal injuries unit in the north east of England over a 5-year period, Spine 30 (2005) 1206–1210. [PubMed: 15897837]

[55]. Sharma HS, Pathophysiology of blood-spinal cord barrier in traumatic injury and repair, Curr Pharm Des, 11 (2005) 1353–1389. [PubMed: 15853669]

[56]. Noble LJ, Wrathall JR, Correlative analyses of lesion development and functional status after graded spinal cord contusive injuries in the rat, Exp Neurol, 103 (1989) 34–40. [PubMed: 2912748]

[57]. Tan HY, Wang N, Li S, Hong M, Wang X, Feng Y, The Reactive Oxygen Species in Macrophage Polarization: Reflecting Its Dual Role in Progression and Treatment of Human Diseases, Oxid Med Cell Longev, 2016 (2016) 2795090. [PubMed: 27143992]

[58]. David S, Greenhalgh AD, Kroner A, Macrophage and microglial plasticity in the injured spinal cord, Neuroscience, 307 (2015) 311–318. [PubMed: 26342747]

[59]. Yang T, Dai Y, Chen G, Cui S, Dissecting the Dual Role of the Glial Scar and Scar-Forming Astrocytes in Spinal Cord Injury, Front Cell Neurosci, 14 (2020) 78. [PubMed: 32317938]

[60]. Bellver-Landete V, Bretheau F, Mailhot B, Vallieres N, Lessard M, Janelle ME, Vernoux N, Tremblay ME, Fuehrmann T, Shoichet MS, Lacroix S, Microglia are an essential component of the neuroprotective scar that forms after spinal cord injury, Nat Commun, 10 (2019) 518. [PubMed: 30705270]

[61]. Zhu G, Wang X, Chen L, Lenahan C, Fu Z, Fang Y, Yu W, Crosstalk Between the Oxidative Stress and Glia Cells After Stroke: From Mechanism to Therapies, Front Immunol, 13 (2022) 852416. [PubMed: 35281064]

[62]. Liu Z, Yao X, Jiang W, Li W, Zhu S, Liao C, Zou L, Ding R, Chen J, Advanced oxidation protein products induce microglia-mediated neuroinflammation via MAPKs-NF-kappaB signaling

pathway and pyroptosis after secondary spinal cord injury, J Neuroinflammation, 17 (2020) 90. [PubMed: 32192500]

[63]. Tam WY, Ma CH, Bipolar/rod-shaped microglia are proliferating microglia with distinct M1/M2 phenotypes, Sci Rep, 4 (2014) 7279. [PubMed: 25452009]

[64]. Guo S, Wang H, Yin Y, Microglia Polarization From M1 to M2 in Neurodegenerative Diseases, Front Aging Neurosci, 14 (2022) 815347. [PubMed: 35250543]

[65]. Rojo AI, McBean G, Cindric M, Egea J, López MG, Rada P, Zarkovic N, Cuadrado A, Redox control of microglial function: molecular mechanisms and functional significance, Antioxid Redox Signal, 21 (2014) 1766–1801. [PubMed: 24597893]

[66]. Simpson DSA, Oliver PL, ROS Generation in Microglia: Understanding Oxidative Stress and Inflammation in Neurodegenerative Disease, Antioxidants (Basel), 9 (2020).

[67]. Petro M, Jaffer H, Yang J, Kabu S, Morris VB, Labhasetwar V, Tissue plasminogen activator followed by antioxidant-loaded nanoparticle delivery promotes activation/mobilization of progenitor cells in infarcted rat brain, Biomaterials, 81 (2016) 169–180. [PubMed: 26735970]

[68]. Rusanescu G, Adult spinal cord neurogenesis: A regulator of nociception, Neurogenesis (Austin), 3 (2016) e1256853. [PubMed: 28405586]

[69]. Kim HJ, Vaziri ND, Contribution of impaired Nrf2-Keap1 pathway to oxidative stress and inflammation in chronic renal failure, Am J Physiol Renal Physiol, 298 (2010) F662–671. [PubMed: 20007347]

[70]. Fawcett JW, Asher RA, The glial scar and central nervous system repair, Brain Research Bulletin, 49 (1999) 377–391. [PubMed: 10483914]

[71]. James ND, Bartus K, Grist J, Bennett DL, McMahon SB, Bradbury EJ, Conduction failure following spinal cord injury: functional and anatomical changes from acute to chronic stages, Journal of Neuroscience, 31 (2011) 18543–18555. [PubMed: 22171053]

[72]. Cao Q, Xu XM, Devries WH, Enzmann GU, Ping P, Tsoulfas P, Wood PM, Bunge MB, Whittemore SR, Functional recovery in traumatic spinal cord injury after transplantation of multineurotrophin-expressing glial-restricted precursor cells, Journal of Neuroscience, 25 (2005) 6947–6957. [PubMed: 16049170]

[73]. Geisler FH, Moghaddamjou A, Wilson JRF, Fehlings MG, Methylprednisolone in acute traumatic spinal cord injury: case-matched outcomes from the NASCIS2 and Sygen historical spinal cord injury studies with contemporary statistical analysis, J Neurosurg Spine, 38 (2023) 595–606. [PubMed: 36640098]

[74]. Liu Z, Yang Y, He L, Pang M, Luo C, Liu B, Rong L, High-dose methylprednisolone for acute traumatic spinal cord injury: A meta-analysis, Neurology, 93 (2019) e841–e850. [PubMed: 31358617]

[75]. Bains M, Hall ED, Antioxidant therapies in traumatic brain and spinal cord injury, Biochim Biophys Acta, 1822 (2012) 675–684. [PubMed: 22080976]

Highlights

- Progressive degeneration of the injured spinal cord exuberates disability over time.
- Oxidative stress at the injury site drives spinal cord degeneration.
- Catalytic intravenously injectable antioxidant nanoparticles mitigate oxidative stress.
- Treatment protects and fosters regeneration, leading to functional recovery.
- As an early therapeutic intervention to stabilize the injured spinal cord.

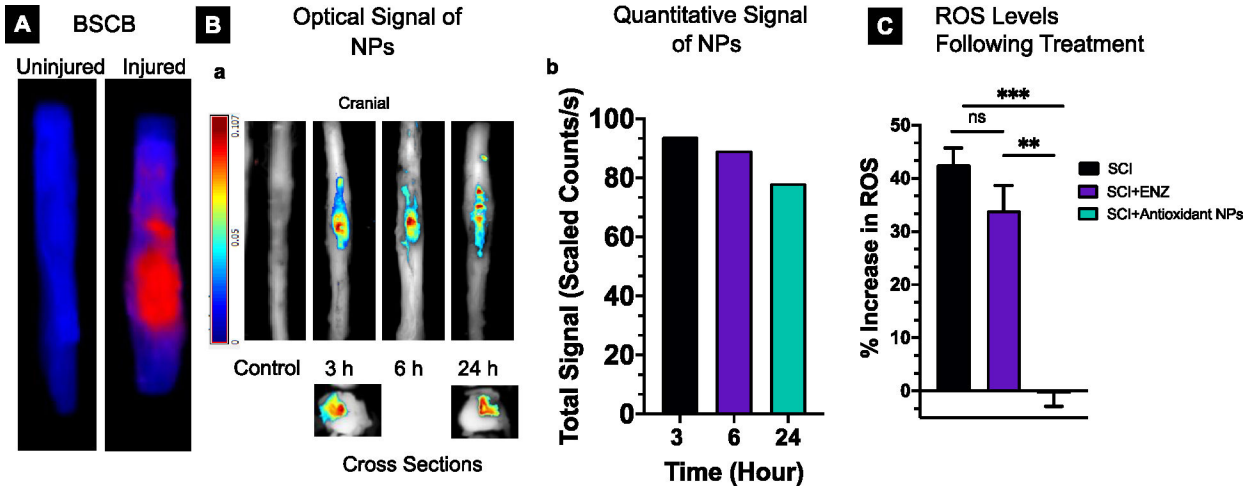

Figure 1. Blood-spinal cord barrier (BSCB) permeability, localization of NPs, and effect of treatment on ROS:

A) Optical images showing the BSCB permeability determined using Evans Blue (EB) dye extravasation method at 24 hours post-injury. **B-a)** Optical images showing localization of near-infrared dye-loaded NPs at the lesion site when they were administered intravenously at different time points post-injury and imaged 24 hours post-administration. Cross-sectional images show the localization of NPs within the lesion cavity. The spinal cord of the animal with injury but did not receive NPs (control) shows no signal; the control spinal cord image reproduced from the previous study [19]. **B-b)** Quantitative signal analysis due to the NP uptake is similar when administered at 3- and 6 hours post-injury but is slightly reduced when administered at 24 hours post-injury. The signal was measured 24 hours after NP administration (n=1). **C)** A single dose of antioxidant NPs (30 mg/Kg) administered at 3 hours post-injury, and the lesion site analyzed at 24 hours post-treatment shows complete neutralization of the post-injury elevated ROS level, whereas an equivalent dose of antioxidant enzymes administered as a solution shows a marginal effect. Percent change in signal due to ROS in the treatment groups was calculated with respect to the signal in the uninjured spinal cord (background signal). Signals were captured using the Maestro Optical Imaging system. SCI (untreated), SCI+ENZ (treated with enzymes in solution), and SCI + antioxidant NPs (treated with antioxidant NPs). Data as mean ± s.e.m. (n = 3). ** $p<0.005$, ***$p<0.0005$

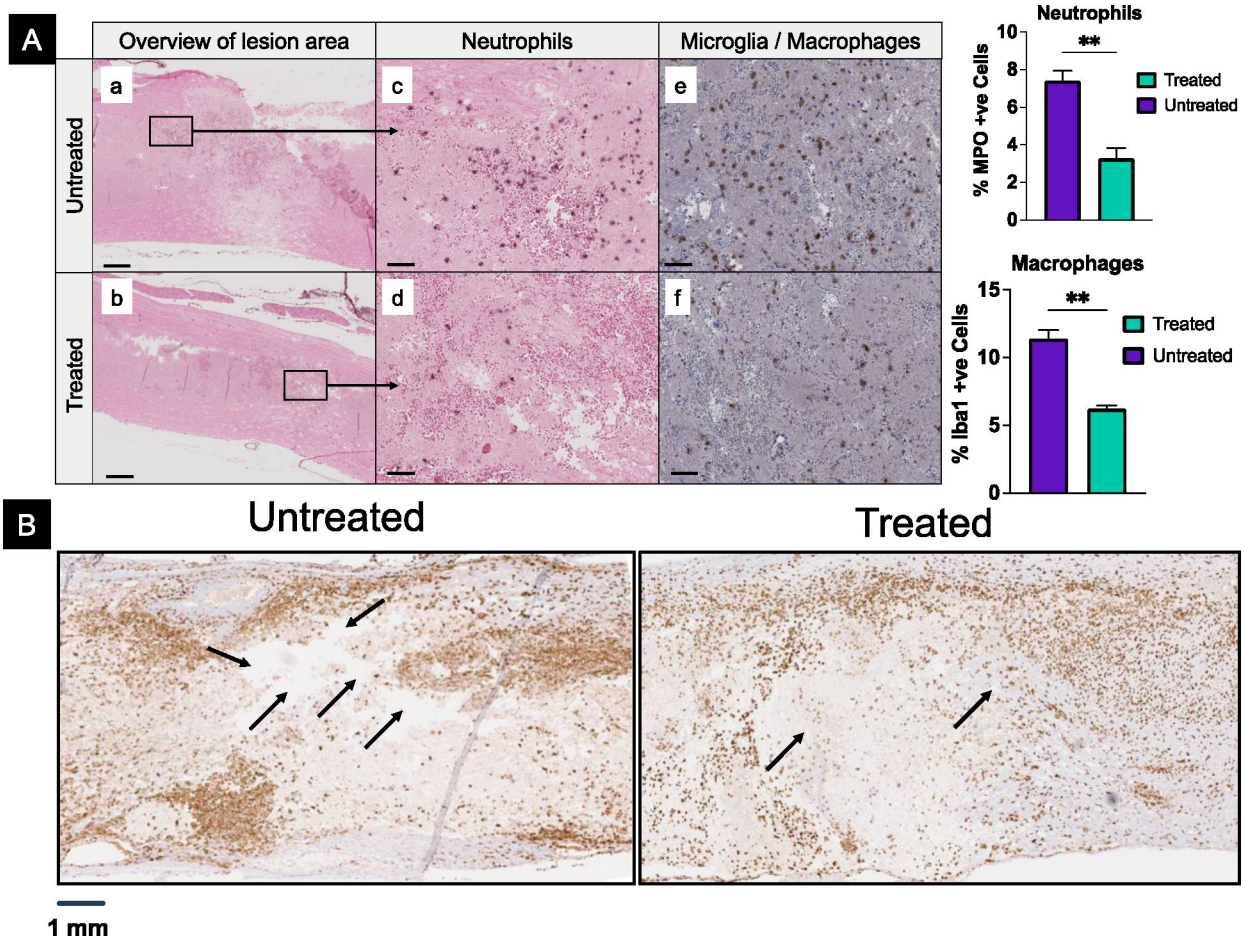

Figure 2. Effect of treatment with antioxidant NPs on early events.

A) Lesion sites in spinal cord tissue at 24 hours post-injury show a significantly lower number of neutrophils (a-d) and activated microglia/macrophages (e, f) in treated than in untreated animals. Macrophages seen are most likely from the circulation. Note-small spherical structures seen in sections are due to RBC. Data as mean ± s.e.m. (n = 3). ** $p<0.005$. Bar =100 μm. **B)** Histological analysis of the spinal cord sections for microglia at 6 days post-injury. In untreated animals, spinal cord sections show large and several cavities (black arrows), whereas these cavities are fewer and smaller in treated animals. Microglia are seen clustering around the lesion site and within the lesion site in treated animals, whereas these are unorganized clusters and very few within the lesion of untreated animals.

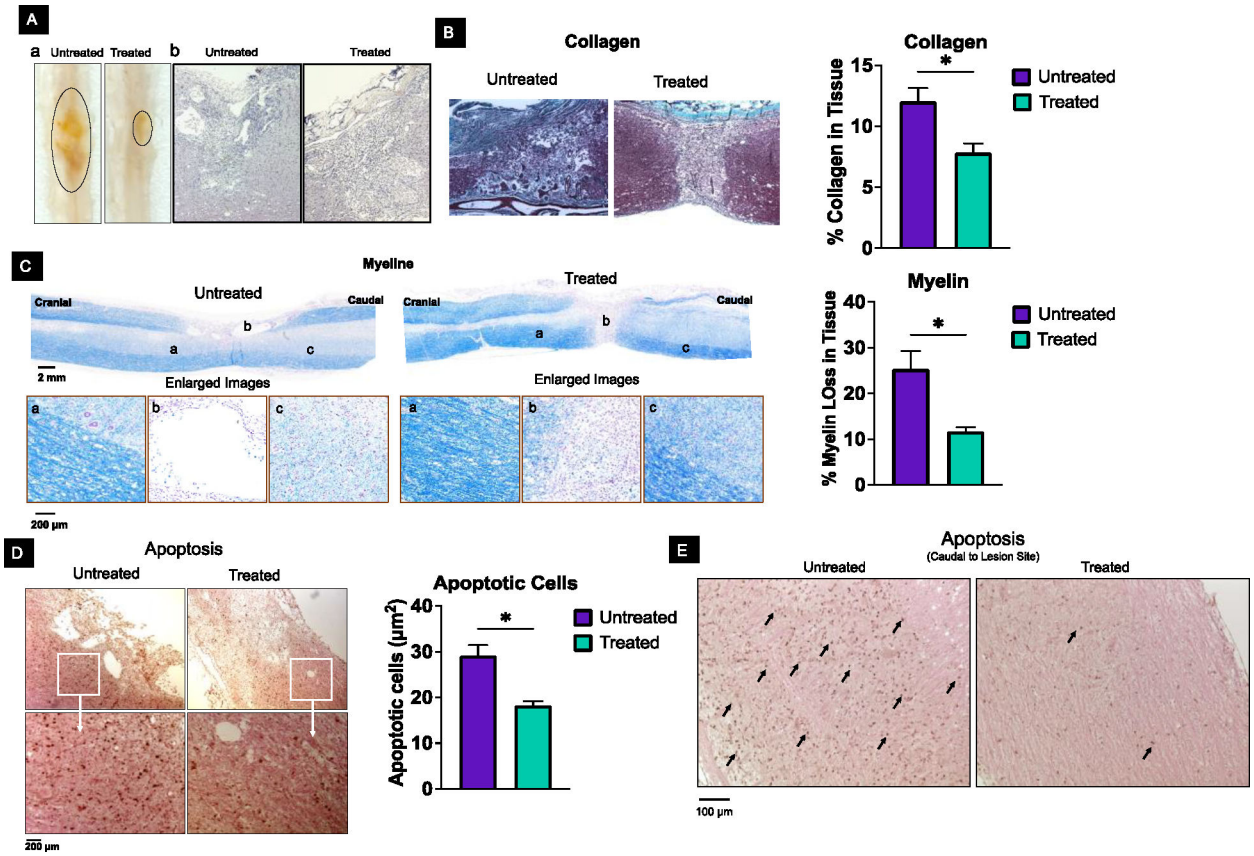

Figure 3. Protective effect of antioxidant NPs and inhibition of scar tissue forming collagen at the lesion site.

A-a) Visual observation of the spinal cords isolated at 4 weeks from untreated animals shows larger lesion areas than from treated animals. A-b) Spinal cord sections from treated animals showed significantly reduced cavitation compared to untreated animals. **B)** Spinal cord sections from treated animals show less collagen (turquoise color) at the lesion site than untreated animals. Note that the strong turquoise color in the spinal cord of treated tissue is not part of the lesion; the dura mater consists of collagen fibers and surrounds the spinal cord. **C)** Analysis of the spinal tissue at 4 weeks shows reduced demyelination of axons in treated than in untreated animals. Percent demyelination was calculated from myelin in the spinal cord section of an uninjured animal. **D)** Spinal cord sections from the lesion site show more apoptotic cells in untreated than in animals. Data as mean ± s.e.m. (n = 3). * $p<0.05$ Bar =100 µm. **E)** Caudal to the lesion site shows more apoptotic cells in untreated than in treated animals.

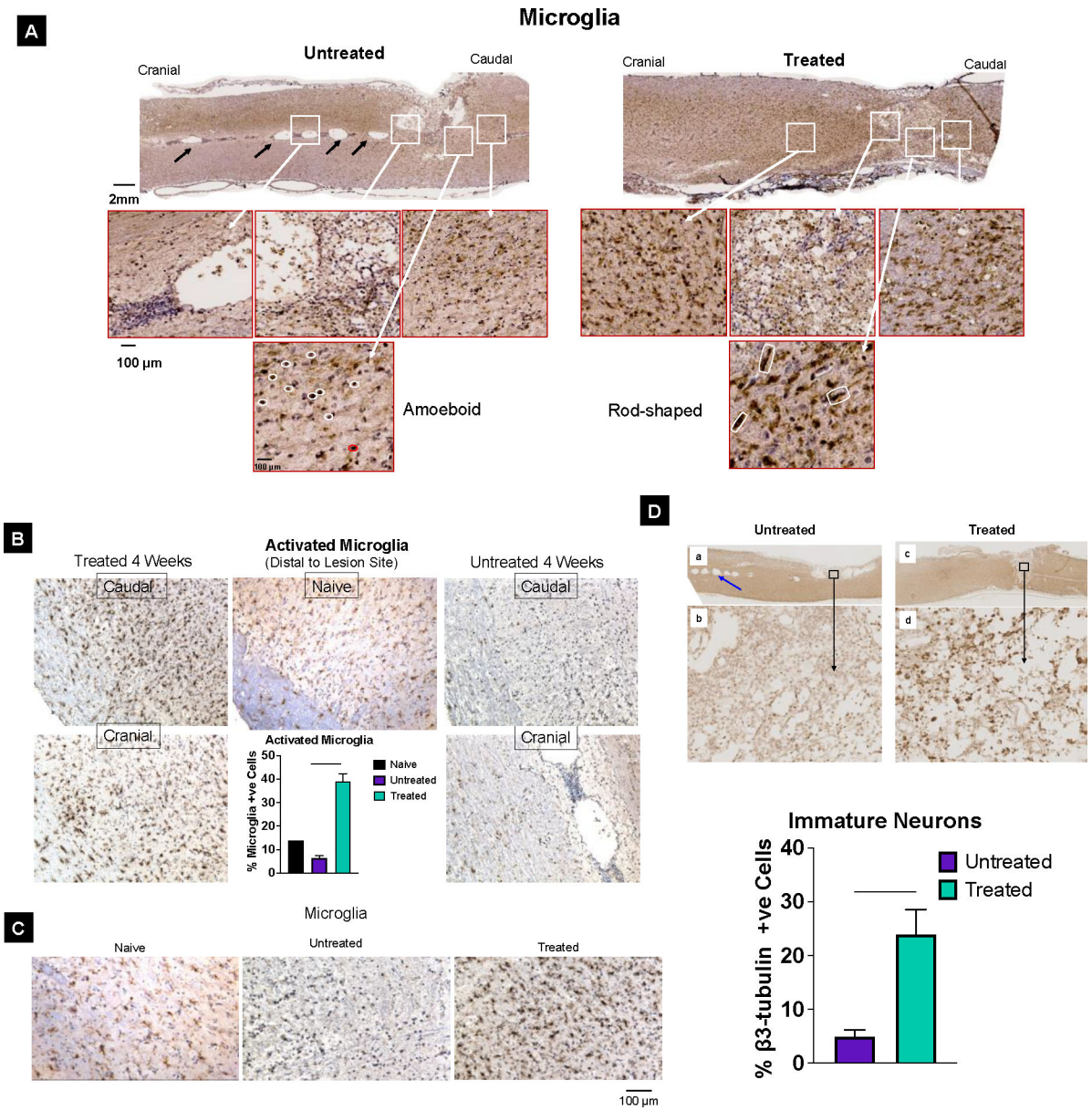

Figure 4. Activated microglia and immature neurons.

A) Syringomyelia are seen in untreated (black arrows) but not in treated animal spinal cord sections. A significant number of activated microglia are seen with signs of healing of the lesion cavity at 4 weeks in treated, but large cavities are seen in untreated animal spinal cord sections. Microglia are amoeboid type in untreated animals (marked in white), whereas they are rod-shaped (marked in white) in treated animal spinal cords (enlarged images). **B)** Microglia from untreated and treated animals' caudal and cranial segments of spinal cord sections. Quantitative analysis shows the number of activated microglia is similar to in naïve control untreated animals but is significantly higher in treated animals. **C)** Magnified images of spinal cord sections showing microglial morphology in Naive control spinal tissue are ramified, whereas, in untreated spinal cord tissue, they appear to be amoeboid type, whereas in treated animal spinal cord sections, they appear to be rod-shaped. **D)** Analysis of the

lesion tissue from treated animals shows the presence of more immature neurons β3-tubulin positive cells than the lesion tissue from untreated animals. Data as mean ± s.e.m. (n = 3). * $p<0.05$; *** $p<0.0005$

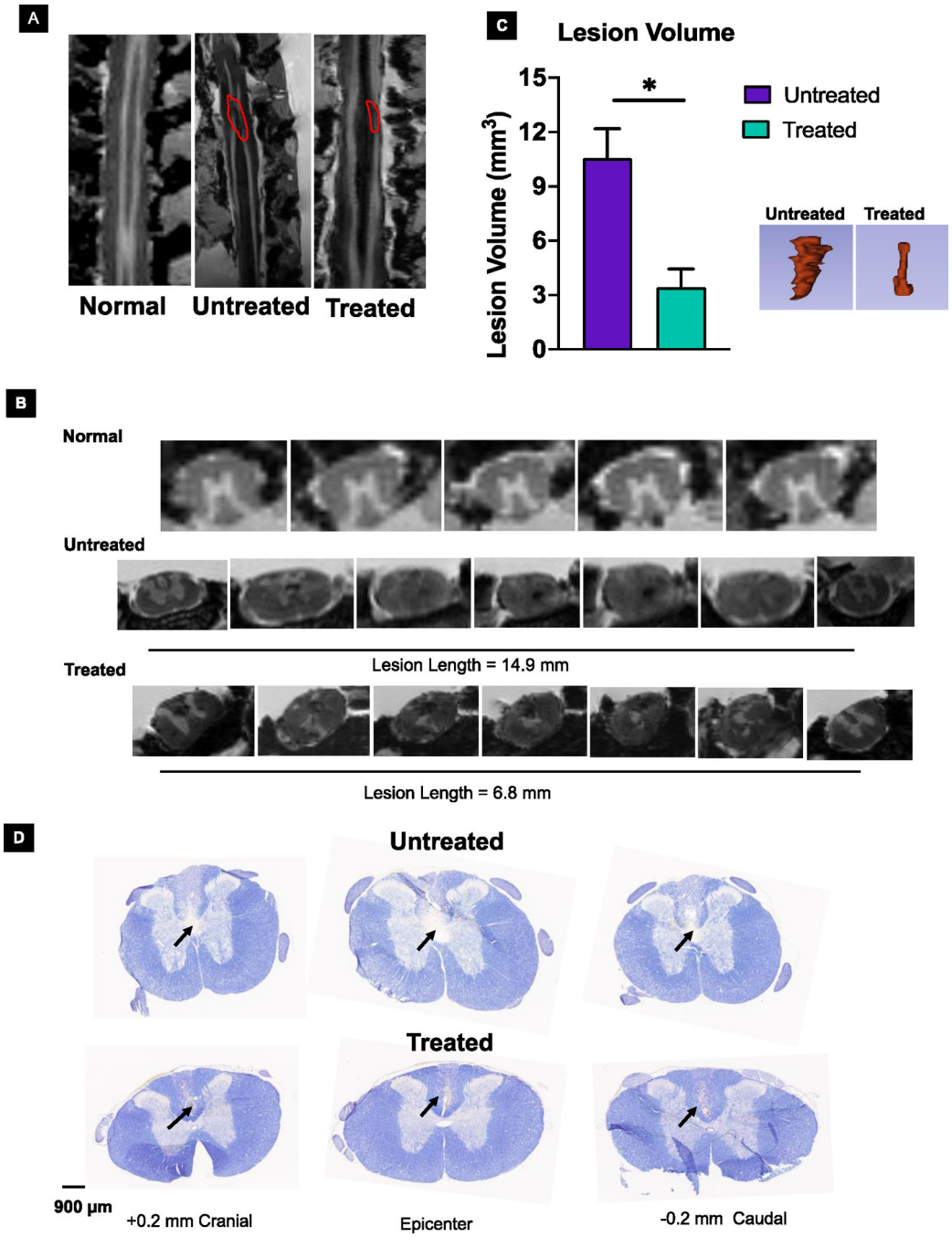

Figure 5. Effect of treatment on lesion volume.

The *in-situ* MRI analysis of the spinal cord at 4 weeks showed reduced lesion volume in treated animals compared to untreated animals. **A)** Marked in red indicates the lesion site. **B)** Lesion length in treated vs. untreated animals (6.8 ± 0.7 mm vs. 14.9 ± 1.6 mm; mean ± s.e.m., n=3, **<0.001). The sections near the epicenter show the presence of grey matter in treated but not in untreated animals**. C)** Quantification shows reduced lesion volume in treated animals compared to untreated animals. Insert: Representative 3D structure of lesion area from treated and untreated animals. Data as mean ± s.e.m. (n = 3). * p<0.05. **D)**

Nissl-stained sections of spinal cords show larger lesion areas from untreated than treated animals

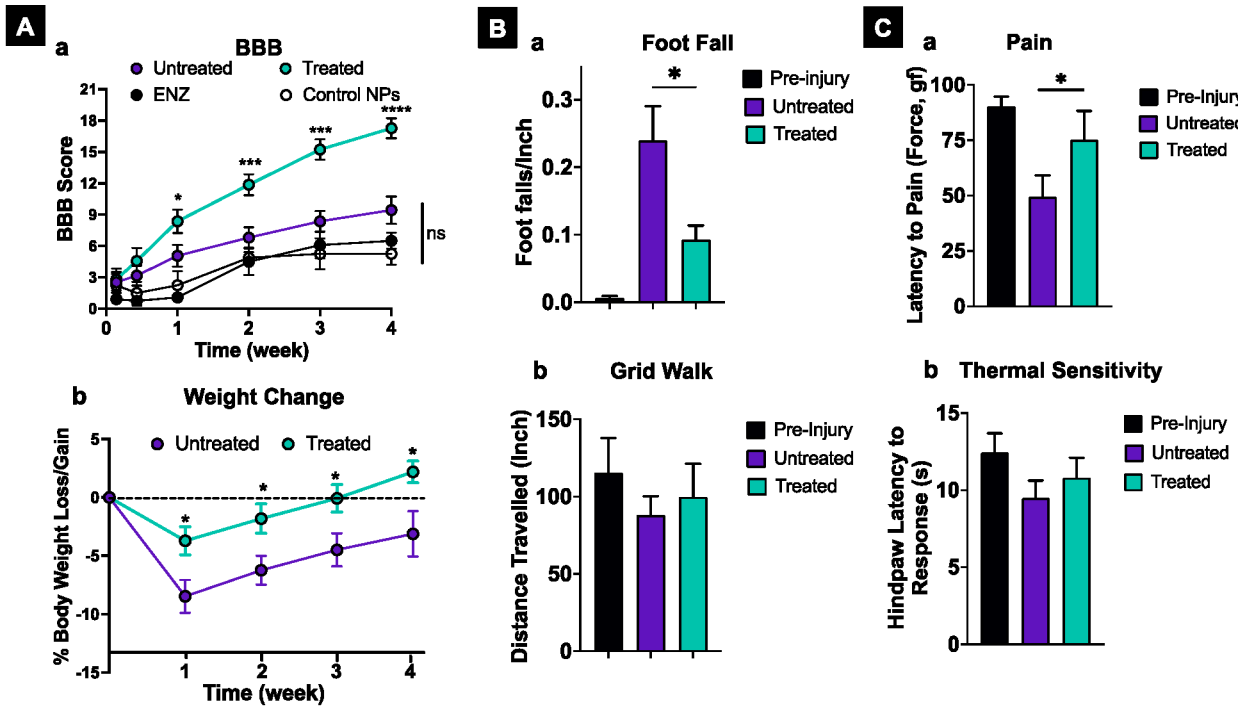

Figure 6. Effect of treatment on locomotive function, body weight, and sensory perception.

A-a) Treated animals demonstrate a steady and significantly greater improvement in the BBB score than controls (untreated, treated with antioxidant enzymes, ENZ, or control NPs). The BBB scores of untreated and treated groups are the compilation of three repeats: treated n=15 M=8; F=7; untreated n=12, M=6, M=6. Other control group studies (ENZ and control NPs) were carried out once, n= 6 (M=3; F=3). **A-b)** Treated animals show lower weight loss post-SCI than untreated animals; also, they gain weight more quickly than untreated animals. n=12, M =6, F=6). **B-a)** Treated animals show lower footfall in the grid walk test than untreated animals. Pre-injury n= 6 M=3; F=3), treated and untreated n=10 M=5; F=5). **B-d)** There was a trend towards animals in the treated group covering more distance in the grid walk test than untreated animals. From both the treated and untreated groups, three animals did not move, and three moved only between 6 to 17 inches. These animal data were not considered in calculating the mean. Pre-injury n= 6 M=3; F=3), treated and untreated n=10 M=5; F=5) (n.s.). **C-a)** In the Randall–Selitto test, treated animals show a higher withdrawal threshold in response to pain than untreated animals. Uninjured n=16 M=9; F=7), treated and untreated =9 M=5; F=4). **C-b)** Treated animals tend to have lower thermal sensitivity than untreated animals. n=13 M=7; F=7). All data shown are mean ± s.e.m. For BBB scoring and body weight change, multiple unpaired t-tests with Welch correction were used to calculate the significance between control groups, ENZ, control NPs, and untreated animals; there was no statistically significant difference between control groups. * $p<0.05$, ** $p<0.005$, *** $p<0.0005$, **** $p<0.0001$.

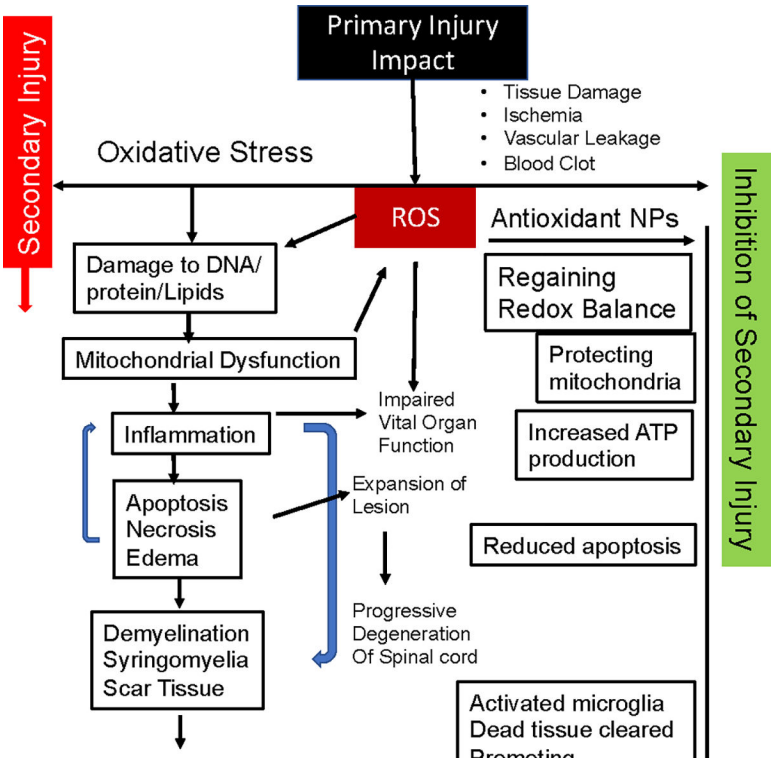

Figure 7. Schematic depicting the mechanism of efficacy of antioxidant NPs.

The initial injury to the spinal cord triggers the ROS-medicated progressive degeneration of the spinal cord, resulting in irreversible changes and permanent disability. Treatment with antioxidant NPs inhibits the cascade of degeneration by neutralizing the effect of ROS and their downstream effects on the degeneration of the spinal cord, thus protecting it from secondary injury progression. The treatment creates conditions in the spinal cord microenvironment to promote healing, resulting in improved functional recovery.

Table 1:

Physical Characteristics of Nanoparticle Formulation

Formulation	Hydrodynamic Diameter (nm)	Polydispersity Index	TEM Diameter (nm)	Zeta Potential mV
Antioxidant NPs	280.2 ± 6.4 nm	0.065 ± 0.005	122 ± 5.5 nm	−17.1 ± 1.5
Dye-Loaded NPs	284.2 ±19 nm	0.11 ± 0.012	ND	−20.7 ± 0.4
Control NPs	270.8± 3.4 nm	0.065± 0.005	ND	−17.6 ± 3.4

Data as mean ± s.e.m., n=3 or more. ND: Not determined